



**Politecnico
di Torino**

Politecnico di Torino

Corso di Laurea Magistrale in Ingegneria Biomedica

A. A. 2022/2023

Sessione di Dicembre 2023

Objective Analysis of Cranial Respiration in Osteopathy

Relatore:
Luca Mesin

Candidato:
Lorenzo Salino

Abstract

This project aims to objectively study the cranial rhythmic motion associated with osteopathy in the cranial field (OCF). To this purpose, several signal analysis techniques have been applied to explore, characterize, and define a possible relationship of the Cranial Rhythmic Impulse (CRI) signal with other biological measurements. Processing was performed on the MATLAB development environment, using a dataset that contained Blood Volume Pulse (BVP), respiration and Intra-Beat-Interval (IBI) measurements, in addition to the CRI signal. The work was structured with a view to find a connection of the CRI signal with the remaining measurements to be able to pave the way for the automation and engineering of the process of skull palpation, which is performed manually to date. A further impetus in approaching this issue with this perspective came from the confirmations that recent studies have given regarding the objective effectiveness of cranial osteopathic therapy. Indeed it came natural, given that the efficacy of this therapy has been confirmed, to look for a link of the CRI signal with other biological signals not only for the reasons mentioned above, but also to better understand its physiological nature. Since the nature of this signal is still not fully known, the analysis of it and the search for its possible correlation with other signals was conducted through various methods, such as peaks analysis, spectral subtraction, anomaly detection with deep learning and Granger's causality analysis. The results obtained from applying the above methodologies to the available dataset unfortunately did not lead to clear results in general. It should be mentioned that a solid correlation was found between the CRI signal and those of respiration and BVP. In particular, the association with the respiration signal, or rather with its abnormalities, yielded first promising cues that seemed to link peaks in the CRI signal with particular trends in the respiratory signal. It was not possible however, even through more in-depth analysis, to confirm the validity of this theory.

Among others, one of the major obstacles encountered was a low signal-to-noise ratio (SNR), whereby noise is meant mainly the interference of the other signals on the CRI, since these had greater strengths. In addition, a ground truth regarding the CRI signal could not be accurately determined from literature, making validation of the various techniques more time-consuming and complex.

Table of Contents

1	Introduction	1
1.1	Literature Review.....	1
2	Background	5
2.1	Clinical Background	5
2.1.1	BVP	5
2.1.2	HRV.....	6
2.1.3	Respiration	8
2.1.4	CRI	9
2.2	Technical Background	11
2.2.1	Time Domain.....	11
2.2.2	Frequency Domain	12
2.2.3	Analog to Digital Conversion.....	14
2.2.4	Fourier Transform	15
2.2.5	Noise.....	16
2.2.6	Filtering.....	17
2.2.7	Correlation	19
2.2.8	Descriptive Statistics	19
2.2.9	F-test	20
2.2.10	Granger's Causality	21
2.2.11	Coherence.....	22
3	Materials and Methods.....	23
3.1	Dataset Acquisition	23
3.2	Dataset Import	24

3.3	Analysis.....	28
3.3.1	Interpolation of HRV	28
3.3.2	BP Filtering.....	29
3.3.3	PSD.....	30
3.3.4	PLV.....	31
3.3.5	Coherence.....	32
3.3.6	Peak Detection on CRI signal	33
3.3.7	Anomaly Detection on RESP signal	37
3.3.8	Granger’s Causality Analysis	40
3.3.9	Spectral Subtraction.....	41
4	Results.....	42
4.1	Visualization of Signals	42
4.2	Filtering.....	44
4.3	PSD.....	45
4.3.1	M-Band.....	46
4.3.2	L-Band	47
4.3.3	VL-Band	48
4.4	PLV.....	48
4.5	Peak Detection on CRI Signal.....	50
4.6	Peak Detection on Respiration Signal.....	53
4.7	Granger Causality	55
4.8	Magnitude Squared Coherence	56
5	Discussion.....	58
5.1	Implications of Results	58
5.2	Limitations and Future Improvements.....	58

List of Figures

Figure 1 ECG (upper plot) and BVP (lower plot) signal.....	6
Figure 2 HRV obtained from R-R peaks measurement from ECG.....	7
Figure 3 Respiration signal	8
Figure 4 Time domain plot of sinusoidal signal	11
Figure 5 Frequency spectrum of sinusoidal signal.....	13
Figure 6 Different types of filters. Upper left corner LP filter, upper right corner HP filter. In the lower part respectively to the left and right BP and BS filter	18
Figure 7 Diagram of Data Import code.....	27
Figure 8 RAW Data Plot.....	42
Figure 9 Temporal detail of signals.....	43
Figure 10 Overall and a detail of filtered CRI signal.....	44
Figure 11 PSD of M-Band signals	46
Figure 12 PSD of L-Band signals.....	47
Figure 13 PSD of VL-Band signals.....	48
Figure 14 PLV of M-Band signals. Computed for CRI and respiration, BVP and HRV respectively.....	49
Figure 15 PLV of L-Band (left) and VL-Band (right) signals. Computed for CRI and RESP, BVP and HRV respectively.	50
Figure 16 Bar diagram of each cluster population	51
Figure 17 Clustering of RESP signal windows, centered on CRI signal peaks.....	51
Figure 18 Clustering of random RESP signal windows.....	52
Figure 19 Output from deepsignalanomalydetector, showing original RESP signal (in blue), reconstructed signal (in yellow) and detected anomalies (in red).....	54
Figure 20 Combined Plot of RESP signal with local minima, as well as CRI signal with local minima and anomaly detected periods.....	54
Figure 21 Time Domain Granger Causality analysis.....	55
Figure 22 MS Coherence averaged over all subjects, relative to signals in M-Band.	56

List of Tables

Table 1: Frequency of TH wave and CRI.....	3
Table 2: Dataset loading performances.	26
Table 3: Different versions of the signals obtained downstream of filtering and downsampling.	30
Table 4 AnomalyDetector models.....	39

List of Abbreviations

Abbreviation	Meaning
CSF	Cerebro Spinal Fluid
OCF	Osteopathy in the Cranial Field
CST	Craniosacral Therapy
PRM	Primary Respiratory Rhythm
CRI	Cranial Rhythmic Impulse
THM	Traube-Hering Mayer
BVP	Blood Volume Pulse
PPG	PhotoPletismoGraph
IR	Infrared
ECG	ElectroCardioGram
HRV	Heart Rate Variability
SNR	Signal-to-Noise Ratio
HR	Heart Rate
CFT	Continuous Fourier Transform
DFT	Discrete Fourier Transform
FT	Fourier Transform
PSD	Power Spectral Density
EM	ElectroMagnetic
LP	Low-Pass

Abbreviation	Meaning
HP	High-Pass
BP	Band-Pass
BS	Band-Stop
ANOVA	ANalysis Of VAriance
H0	Null Hypothesis
Ha	Alternative Hypothesis
CPM	Cycles per Minute
EMG	ElectroMioGraphy
IBI	Inter Beat Interval
NaN	Not a Number
STD	STandard Deviation
FIR	Finite Impulse Response (filter)
PLV	Phase Locking Value
ADF	Augmented Dickey-Fuller
KPSS	Kwiatkowski, Phillips, Schmidt e Shin (test)

1 Introduction

In an era where holistic healthcare approaches are gaining recognition and importance, this master's thesis embarks on a journey to explore the possibilities that an engineering approach could give to cranial manual therapy.

Osteopathy is a practice with more than a hundred years of history: its first principles were the outcome of the work of A.T. Still in the late 19th century. In the following years many others showed interest in this new way of treating diseases and became students of Still. One of them was W. G. Sutherland, which then dedicated his life to a particular branch of osteopathy that focused on the cranium.

One key aspect on which osteopathy, as well as other holistic approaches are based upon, is the subjectiveness of measurements and the absence of analytical or statistical data manipulation. One of the main goals of this work is to address this lack of objectiveness by exploring with state-of-the-art signal analysis techniques various biometric signals that could give objective references to cranial manual therapy, and possibly decouple measurement from human error.

This work will therefore follow an exploratory approach, starting from the analysis of the available literature, and then proceeding to the processing of the available data through different signal analysis techniques in the MATLAB development environment.

1.1 Literature Review

According to the research made by W.G. Sutherland, cranial bones are beveled for articular mobility to accommodate the motion of a respiratory mechanism, which also propagates to the sacrum via CSF (Cerebro Spinal Fluid) and can be palpated throughout the whole body. This respiratory mechanism, according to Sutherland, is a minute motion that occurs between the different bones of the skull. He published his ideas in 1939 in a book called *"The*

Cranial Bowl"¹, after 40 years of research. Since then, the key components of the **OCF** (Osteopathy in the Cranial Field) have not changed much.

The technique used by OCF practitioners goes under the name of **CST** (Craniosacral Therapy) and the concept behind it is that by manipulating the bones and tissues of the skull a variety of health issues can be improved.

Practitioners of OCF use as guidance a rhythmic pulse that they sense from the palpation of the skull of the patients. Therapy sessions start with the specialist establishing a "fulcrum point" with their forearms or elbows on the treatment table. They then position both hands around the patient's head, apply a gentle pressure (which is very variable) and sense the pulse. They do not exert this force directly with hands but through the fulcrum point.

Being based on the feeling of each practitioner, to this day there are no generally accepted quantitative measures of these rhythmic pulse, called PRM (Primary Respiratory Mechanism) or CRI (Cranial Rhythmic Pulse).

Patients report to feel a "pressure release" during and after these treatments, but until now no clinical evidence has been found to support this practice. Many experts in the medical field are skeptical even to the fact that this therapy can bring effective benefit to the patients, and sustain that positive sensations are just a placebo effect. Regarding this matter, Haller et al.² demonstrated in 2016 that CST is indeed an effective and safe way to reduce neck pain.

In 1999, the first comprehensive study of the CST has been commissioned to the BCOHTA (British Columbia Office of Health Technology Assessment), that unfortunately was not able to find evidence to support the benefits that CST patients reported³.

Another important step forward in the comprehension of the PRM was made in 2001 by Nelson et al.⁴. Starting from the available data of another whole-body phenomena, the Traube-Hering Mayer wave (THM), the team investigated for a possible correlation with the PRM. Using laser-Doppler flowmetry they were able to develop a protocol to measure THM

and PRM simultaneously and discovered a statistically significant correlation between palpated CRI and the lower frequency of the measured THM wave.

Conclusion of this study was that THM oscillation and PRM were strictly connected and may even be the same thing. Further investigations done by Nelson’s group in 2006 ⁵ demonstrated a 1:2 ratio in PRM and THM frequency between palpation and instrumental recordings. Considering all the low-frequencies phenomena (in the PRM spectrum of 6-9 cpm) that happen in the human body, the team concluded that to arbitrarily associate PRM with one of these was an oversimplification, and further study had to be done.

Phenomena	Frequency (mean ± STD) in cpm
TH wave	9,91 ± 3,03
PRM (palpated)	5,39 ± 2,20

Table 1: Frequency of TH wave and CRI

Interexaminer reliability has also been the focus of few studies ⁶⁻⁸, as in most cases tends to be poor to absent. Slightly better results are obtained where repeated measures are made from the same practitioner, suggesting that the hypothesis made from Hamm ⁹ could have solid foundations: if the PRM is effectively altered by the contact between the patient’s head and the practitioner’s hands many contact variables, that are different for each osteopath, assume much more weight in the composition of the PRM.

Another study ¹⁰ carried out on children with infant colic shows that a complete resolution of symptoms can be obtained on day 24 of therapy by receiving 1 to 3 sessions of CST compared to the control group that received no treatment. However, it should be emphasized that it is not known what the differences in the number of sessions depend on: according to the study, this variability could depend on the type of birth, but it is possible that some children were close to spontaneous recovery.

As many other practices in history that improved people’s health, CST quickly became widespread and to this day, as supported by different studies ^{2,11,12}, represent a valid

alternative to improve many pathological issues. It therefore safe to say that OCF to this day has made a positive impact in the lives of many, but there is still no unique explanation to the mechanism behind it.

On the other hand, it is important to make the scientific community aware of the possible adverse events that could be correlated to forced CST in some patients: even if up to this day CST proved to be as safe as other manipulative treatments ⁶⁻⁸, no recommendations about pain conditions have been made.

It is consequently called for to continue the scientific analysis to find more about the physiological processes that are involved. Further understanding of the mechanism behind OCF would open much more advanced therapy possibilities, such as automated sessions and an engineering approach to the matter. By instrumentally evaluating physiological parameters, many variables could be adjusted in a much more precise way, therefore enabling both practitioners and eventually automated systems to improve therapy outcomes.

2 Background

This chapter will cover some basic information about the biological signals that this work is based on, as well as some knowledge regarding the concepts behind some signal analysis techniques that will be explained in the “Materials and Methods” section.

2.1 Clinical Background

2.1.1 BVP

“BVP” stands for “Blood Volume Pulse” and it is a physiological signal characterized by the pulsatile flow of blood. It can be measured in different regions of the body, typically using a non-invasive technique called Photoplethysmography (PPG).

This technique exploits the variations in the diameter of the arteries, which contract and expand following the change in blood pressure caused by heartbeats. This pulsatile behavior is detected using a PPG sensor, that makes use of low-intensity infrared (IR) light. The device is composed of a light emitter and a receiver, and the signal that it gives as output is proportional to the intensity of the light ray that is not absorbed by the tissues between the emitting and the receiving part of the sensor. Light is more strongly absorbed by blood than the surrounding tissues, and this enables to relate the output signal of the device to the fluctuation of blood pressure in the blood vessels.¹³

This technique offers more than one advantage: it is both cost effective and non-invasive, and most of all it is applicable to a wide range of body parts, such as fingers, forehead, nasal septum and ears, making it very versatile. It should be noted that PPG devices require precise calibration, as the quality of the signal acquired is extensively dependent from the contact force and the site of measurement.

As shown in Figure 1, BVP signal morphology resembles the ECG: both shares a dominant frequency, corresponding to the heart rate. Each pulse wave typically has two main components: a systolic upstroke and a diastolic downstroke.

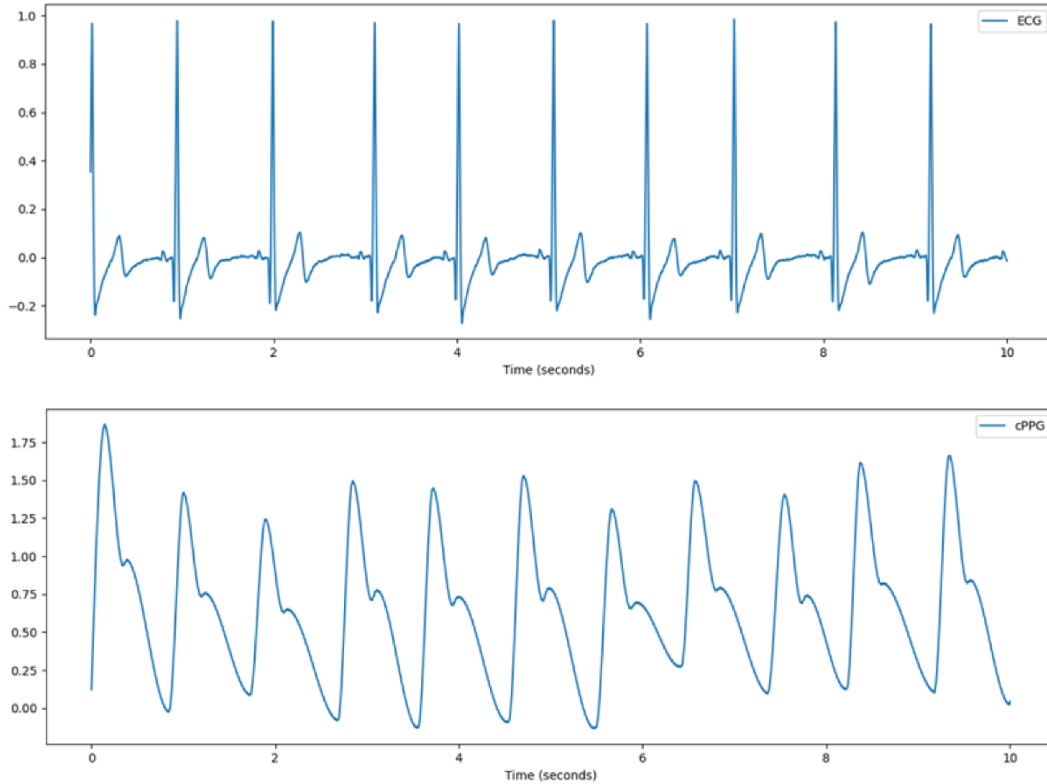


Figure 1 ECG (upper plot) and BVP (lower plot) signal

The applications in which the BVP signal is used today range widely: blood oxygen saturation, arterial compliance and ageing, autonomic function monitoring, blood pressure, heart rate, etc.

In this work the BVP signal will be used also to obtain information regarding the Heart Rate Variability (HRV).

2.1.2 HRV

The Heart Rate Variability (HRV) is a signal that quantifies the time interval between two consecutive heartbeats. It's increasingly of great importance in the study of the autonomic system and in the assessment of cardiovascular health.

In order to precisely measure the time between two heart pulses, the easiest and most effective way has been proven to be the measure of the R-R interval from an ECG record. A single ECG waveform is in fact divided in three main components:

1. P-wave: indication of atrial depolarization (contraction).
2. QRS complex: highest part of the waveform in amplitude, corresponding to the ventricular depolarization.
3. T-wave: terminal part of the ECG undulation, representing the ventricular repolarization.

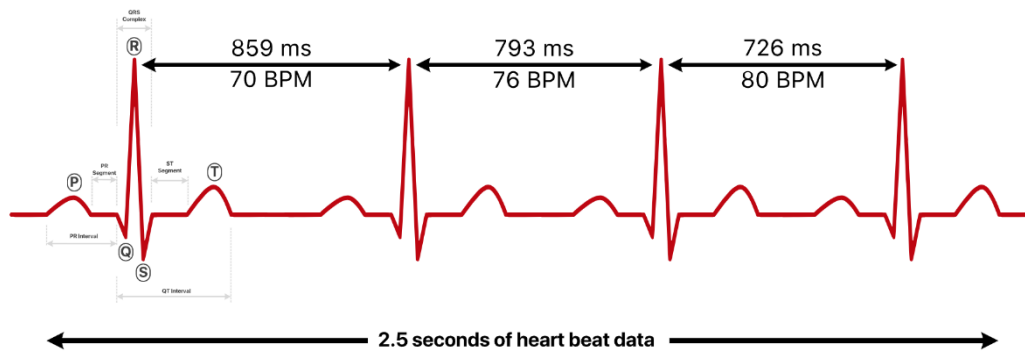


Figure 2 HRV obtained from R-R peaks measurement from ECG.

Since the R marker represent the highest-amplitude point, it's easy to deduce that it is also the part of the ECG wave with the highest SNR, making it the most used reference by algorithms to compute the time interval between heartbeats.¹⁴

Also, is possible to calculate the HRV signal from a BVP record, as the latter shows a similar morphology to the ECG: the ventricular contraction translates as a prominent peak also detectable by PPG sensors. It should be noted that the extrapolation of heart rate variability from the blood volume pulse is not as precise as it is with the ECG signal.

The interest in this signal has become greater in the recent years as its clinical significance has been proven in various aspects. In particular, the HRV signal is widely used in the analysis of the autonomic system, as well as in the assessment of cardiac health.

To extract useful information from this signal, there are two main approaches:

- Time-domain analysis: in which statistical measures such as standard deviation are calculated from temporal variables.
- Frequency Domain analysis: the HRV track is divided in several frequency bands that are then studied both individually and in groups, determined from the processes that each of them influence.

Since the HRV is not obtained via direct measure, but it is instead derived from other signals, its interpretation can be complex, due to possible interferences and other unpredictable factors.

2.1.3 Respiration

Breathing is one of the fundamental physiological functions of our organism. It is responsible of the acquisition of oxygen and the disposal of carbon dioxide (CO₂). In rest conditions, an adult has a respiration rate comprised between 12 and 18 breaths per minute.¹⁵

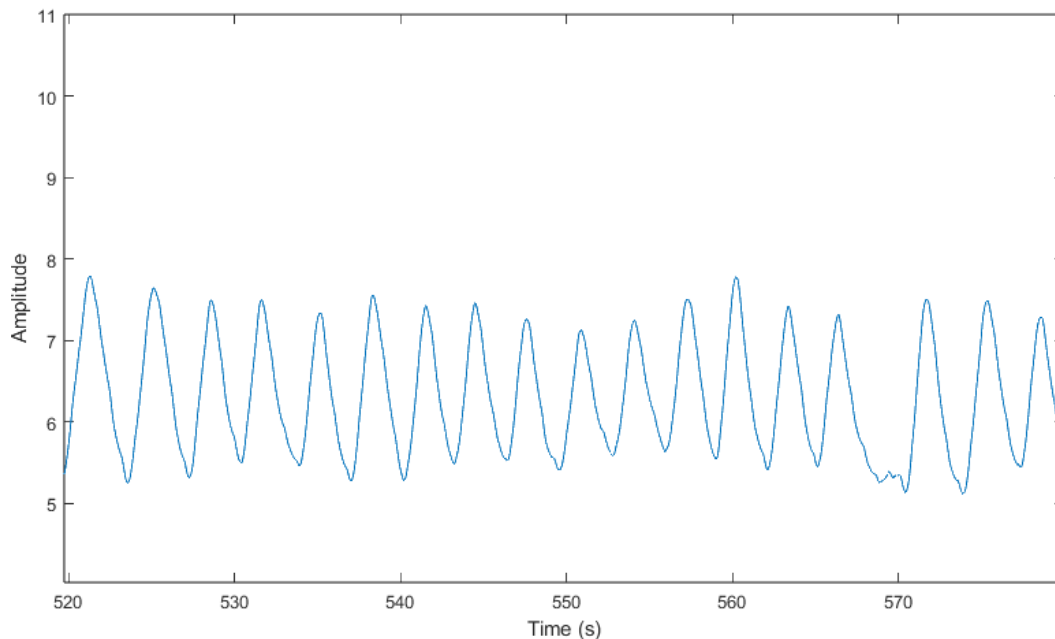


Figure 3 Respiration signal

Beside from visual and auditory evaluation, breathing functionality can be also evaluated with numerical analysis of a signal obtained by direct acquisition or extrapolation from other biometrical measures. Indirect methods are commonly based on the ECG or Heart Rate (HR) signal, depending on the level of detail and precision that is necessary to achieve.

In direct non-invasive methods, the acquisition takes place by placing a strain sensor under the rib cage during respiration. As the person inhales and exhales, the sensor gives different output voltages, as shown in Figure 3.

2.1.4 CRI

In the past few decades, many researchers tried to measure objectively the aforementioned “pulse”, called PRM/CRI. None of the numerous studies has been able to give a definitive physiological explanation to this pulse. Nevertheless, major steps forward have been made in the understanding of it.

In particular, one of the first attempts to record the CRI with scientific instruments was made by Viola M. Frymann¹⁶ in 1971, using a pair of captators. Since the common reference for motion in this configuration was the treatment table, the team also had to develop a structure to minimize movement of the subjects without affecting the freedom of the practitioner in his hand positioning. This was achieved by combining a specially designed neck rest to a small sandbag (to cancel breathing motions) and by positioning the pick-offs on opposite sides of the skull (to cancel displacement of the head).

The contralateral sensors were suspended by high quality springs to avoid effects of external vibrations. The tips of those sensors had to be progressively tightened to compensate the tissue deformation underneath them and keep a constant and firm pressure on the subject. Pickoffs used are matched differential transformers in opposing series, to cancel the head displacement and simultaneously double the desired pulsatile signal.

Frymann et al. successfully recorded a cranial motion and were able to demonstrate that it was not correlated to cardiac or respiratory pulses. The recordings showed a range of motion of 1,96 - 3,93 μm .

In 2021 a new attempt at measuring the PRM (called also “third rhythm”) was made by Rasmussen et al.¹⁷ The set-up of this experiment resembled in some way the work done by Frymann et al. in 1971, but with different sensors: in this case two servo actuators were placed on the temporal mastoids with 10g of contact pressure.

Measurements were made on 50 healthy subjects, showing consistently a third rhythm not correlated with arterial and respiratory fluctuations. The mean frequency was 6,16 cpm (4,25 – 7,07). The team proposed that this fluctuation could be related to the balance of the autonomic system.

Equally important as the quantitative measure of the PRM, is the physiological source of this phenomena. In his study, Hamm⁹ tried to address this question. He proposed that the application of manual compression from the practitioner hands to the patient’s head may cause a net negative charge in the collagen matrix, changing its state from gel to sol. Also, another hypothesis he made is that the same ionic movement that causes the negative charge could alter the H^+ and Ca^{2+} distribution and thus creating an electrochemical gradient. This charge could change the thixotropic properties of the collagen and stimulate a vasomotive response, that would explain how practitioners can (either voluntarily or involuntarily) alter the THM / PRM of their patients during therapy sessions. Also, this mechanism could explain the high interexaminer variability that every study tends to register.

2.2 Technical Background

In this section some basic principles of signal analysis will be covered, to better understand the following chapters that will cover in detail the steps made during the analysis work.

2.2.1 Time Domain

In signal analysis, the time domain is one of the two primary domains used to analyze and represent signals, with the other being the frequency domain, which will be discussed in the next subsection. The time domain focuses on the behavior of a signal as a function of time. It provides information about how a signal changes over time, which is essential for understanding its temporal characteristics.

The signal representation as a function of time shows how the signal's amplitude (or value) changes at each instant in time. It is often denoted as $x(t)$, where "x" represents the signal, and "t" represents time.

A common way to visualize data in time domain is usually by representing time on the horizontal axis (x-axis), and the signal's amplitude on the vertical axis (y-axis), as shown in Figure 4. This allows to see how the signal varies over a specified time interval. This is the form that time domain plots will have throughout this work.

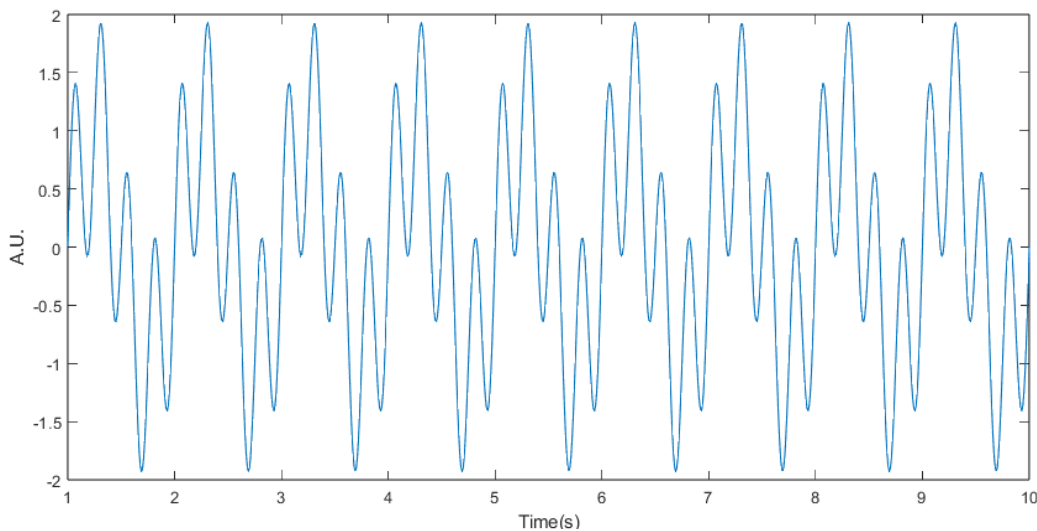


Figure 4 Time domain plot of sinusoidal signal

By analyzing a signal in the time domain, it is possible to determine various characteristics, such as its duration, amplitude, and shape. Some of the most common measures that are made in this domain are peak amplitudes, average values rise and fall times, as well as standard deviation.

Signal processing operations such as differentiation, integration, and time shifting are also typically performed in the time domain. These operations allow to manipulate and modify signals to extract or enhance specific features.

Also, in time domain is possible to evaluate and analyze short-duration events like transient or anomalies, especially when dealing with signals that exhibit mostly regular behavior.

2.2.2 Frequency Domain

While the time domain provides valuable insights into a signal's temporal behavior, the frequency domain, which involves techniques like Fourier analysis, helps reveal the signal's frequency components and spectral characteristics.

The frequency domain provides insight into the frequency components that make up a signal, allowing us to understand how different frequencies contribute to the overall signal's behavior. This domain is particularly useful for studying periodic or oscillatory phenomena and is widely employed in fields such as electronics, audio processing, communications, and many other scientific and engineering disciplines.

In this domain, a signal is represented as a sum of sinusoidal components of varying frequencies and amplitudes. Mathematically, this representation is typically expressed as a sum of sine and cosine functions at different frequencies. The signal can be denoted as $X(f)$, where "X" represents the signal in the frequency domain, and "f" represents frequency, as shown in Figure 5. The spectrum shown in the preceding mentioned figure is calculated from the signal of Figure 4.

Commonly used is a graphical representation that shows the amplitude of each frequency component in the signal called “frequency spectrum”. It displays how the signal’s energy is distributed across different frequencies. The most common tool for visualizing the frequency spectrum is the Fourier Transform.

The aforementioned is a mathematical technique used to convert a signal from the time domain to the frequency domain. It decomposes a signal into its constituent frequency components, providing information about the amplitude and phase of each frequency. There are two variations of this transform: the Continuous Fourier Transform (CFT) and the Discrete Fourier Transform (DFT). The first is used for continuous-time signal, which can be obtained via analog acquisition, while the latter is used for discrete-time signals, such as digital ones.

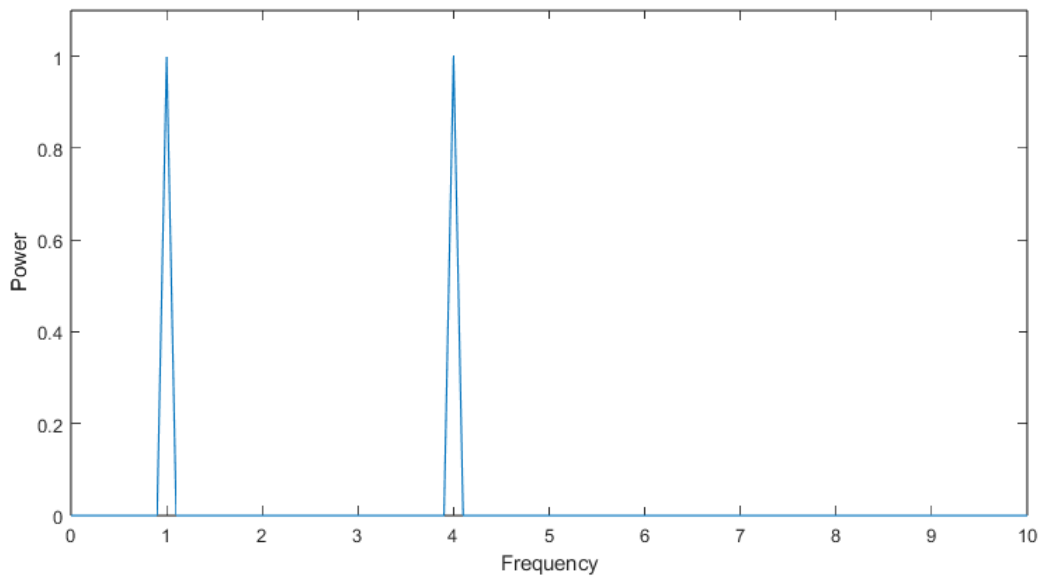


Figure 5 Frequency spectrum of sinusoidal signal

2.2.2.1 Power Spectral Density

The Power Spectral Density (PSD) is a measure of how the power of a signal is distributed across different frequencies, as shown in Figure 5. It quantifies the strength of each frequency component and is often used to characterize the frequency content of a signal.

After evaluation of the spectral composition, it is possible to further analyze signals in the frequency domain and then convert them back to the time domain, using the Inverse Fourier Transform. This reconstructs the original signal from its frequency components.

The frequency domain is essential for various applications, including audio processing (e.g., equalization and filtering), image processing, wireless communications (e.g., modulation and demodulation), and the analysis of complex systems with multiple interacting signals. It complements the time domain analysis and is a powerful tool for understanding the characteristics of signals and systems in a different perspective.

2.2.3 Analog to Digital Conversion

With the introduction of digital technologies, the world of signal analysis undertook a significant change: the computational power unlocked with these devices opened countless possibilities in the field.

In order to assess the large amount of algorithmic potential, the information must be converted in a form that is manageable by these digital devices. Time, for instance, could be seen by human beings as a continuous variable: units of measure of different orders of magnitude help us to measure it, but as long as there is capability to think of smaller units, the resolution of a specified block of time can be improved. Digital devices are instead capable only to represent data up to a specified resolution.

The continuous data recorded from a generic type of sensor must be converted to discrete values in order to be stored and accessed from digital devices. This process is called **sampling** when it is done on time variables, and **quantization** when is done on amplitude variables.

In particular, the sampling process is done by taking measurements of the continuous-time signal at specific intervals, the frequency of which is known as **sampling rate** and measured in Hz. Audio signals, for example, are commonly sampled at 44100 Hz, meaning that between each data point there is an interval of $22,67 \mu\text{s}$.¹⁸

Choosing the correct sampling rate is a fundamental step in the analog-to-digital conversion process. Clearly the sampling rate must be high enough to give a faithful representation of the applied signal. In particular, Nyquist's theorem states that a periodic signal must be sampled with sampling rate at least twice the highest frequency component of the signal. In the aforementioned example, the highest frequency that can be represented would be 22050 Hz.

Another process similar to the one described above, known as **quantization**, has to be performed to convert the continuous amplitudes to discrete values.¹⁸ This procedure determines the resolution of the signal, in terms of its specific unit. Digital devices, as mentioned before, are capable of a predetermined level of precision, nowadays determined by the number of bits that are available to store each sample of the signal: to work in the most effective way possible, it is of great importance to establish a priori the amplitude range of the signal that has to be quantized. By doing so, it is then possible to map continuous amplitude values within the range to a finite set of discrete values, accordingly to the machine precision of the device.

2.2.4 Fourier Transform

Among all transforms used in signal and image processing, Fourier transform (FT) is probably the most used. The formal definition for 1-D continuous FT is defined as follows:

$$G(f) = FT\{g(t)\} = \int_{-\infty}^{+\infty} g(t)e^{-j2\pi ft} dt$$

Where:

1. $g(t)$ is the continuous time signal.
2. $G(f)$ is the resulting function in the frequency domain.
3. t is the time variable.
4. f is the frequency variable (expressed in Hz or multiples).

5. j is the imaginary unit

This mathematical operation allows to move from the time domain to the frequency domain, without loss of information.¹⁹ It is one of the fundamental tools used in digital signal (and image) processing, in its discrete form (DFT – Discrete Fourier Transform).

Exploiting the preserved integrity of information, it is possible to apply the inverse transform and move from the frequency to the time domain:¹⁹

$$g(x) = IFT\{G(f)\} = \int_{-\infty}^{+\infty} G(f)e^{j2\pi ft} df$$

2.2.5 Noise

Most biomedical signals appear as weak signals in an environment that is teeming with many other signals of various origins. Any signal other than that of interest could be termed as an interference, artifact, or simply **noise**.

Due to the high amplification factors needed to obtain readable signals from biological phenomena, noise sources are almost countless: for example, electronic noise from instrumentation is not negligible in this field, as it gets amplified with the same factors as the desired signal. The thermal component of this noise can be partially reduced with appropriate cooling solutions, that may not be always suitable.²⁰ Other relevant noise sources are EM fields (both natural and man-made), upon which the 50-60 Hz power supply interference is particularly well-known.

The removal of these impurities in a particular signal represent in most cases one of the first steps of signal processing.

Unfortunately, noise is not a deterministic signal, hence its value is not predictable from the knowledge of past values or via a mathematical function. This kind of waveform are labeled as **nondeterministic** or **random signals**. The classification of a signal as deterministic or nondeterministic is not based on subjectiveness, although random waveforms are expected

to have more excursion both in frequency and amplitude with respect to a predictable signal with comparable reference level. Kendall, Challis and Kitney proposed a randomness test based upon the number of peaks and/or troughs in a specified interval.^{21,22}

2.2.6 Filtering

To overcome the numerous problems created by noise, as well as to enhance, extract or suppress certain parts or features of a signal, **filtering** is employed.

The primary goal of signal filtering is to enhance, isolate, or remove certain frequency components or noise from a signal. Depending on the desired effect, different types of filters may be applied:²³

- **Low-Pass (LP):** this type of filter keeps low-frequency components of the signal intact, while suppressing all frequency components higher than a predetermined threshold. This filter is most suitable for noise removal, as this type of interference is usually located at high frequencies. Furthermore, LP filters are also widely employed to smooth signals.
- **High-Pass (HP):** this kind of filter, opposite to the preceding one, allows high frequency components to pass, while attenuating low-frequency components. Its main application is in feature extraction or low frequency noise removal.
- **Band-Pass (BP):** this class of filters combines the two previous ones mentioned, allowing only a specific band of frequency to pass, suppressing all the remaining spectrum. A typical use case for this kind of filter is in isolating a narrow-band signal buried in noise.
- **Band-Stop (BS):** this model of filter provides the opposite effect of the antecedent. It is most useful to isolate and suppress noise or interference when located in a different frequency band from the desired signal.

- **Notch Filter:** this filter can be considered as a band-stop filter with a very narrow stopband, that can be centered even around a single frequency. Its most widespread application is the removal of 50 or 60 Hz powerline interference.

In Figure 6 are depicted the different types of filters mentioned above.

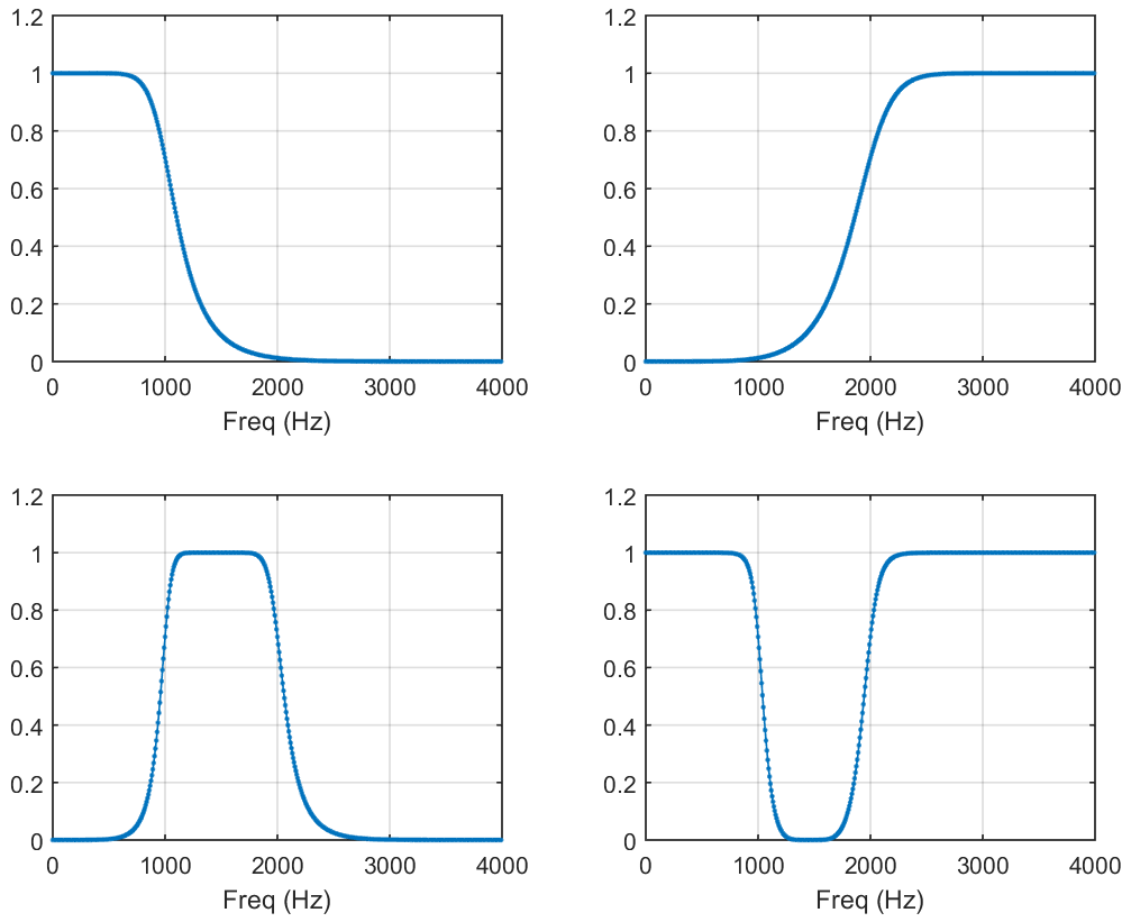


Figure 6 Different types of filters. Upper left corner LP filter, upper right corner HP filter. In the lower part respectively to the left and right BP and BS filter

Aside from the type of filter, there are some other important parameters that define the behavior of these algorithm and devices. Among others, the main characteristics that determine a filter are:²³

- **Filter order:** this parameter indicates the number of poles that are present in the filter's transfer function. Higher-order filters allow more significant changes to the signal but have greater computational cost.

- **Cutoff frequency:** this specification defines the frequency or frequency band in which the filter works. For LP, HP and Notch filters a single frequency is specified, while in BP, BS filters this parameter comprehends two numbers.
- **Filter Gain:** This variable determines the amplification or attenuation applied by the filter to the specified frequencies.

2.2.7 Correlation

When dealing with non-stationary processes, as many biomedical signals can be defined, it may result very challenging to assess resemblance between two streams of information. This problem is often overcome using the correlation mathematical function: it discovers the similarity between two signals by considering a possible shift in time. The following is the formula used to calculate correlation:

$$R(\tau) = \int_{-\infty}^{+\infty} x(t)y(t - \tau)p_{x,y}(x(t), y(t - \tau)) dt$$

There are two primary types of correlation:

1. Cross-correlation: it measures the similarity between two different signals, and it is most used to determine eventual delays, common patterns or general relationship.
2. Autocorrelation: used mainly to determine pattern or periodicity of a signal. It is calculated using the same function quoted above but replacing $y()$ with $x()$.

2.2.8 Descriptive Statistics

In the vast field of statistics analysis, there are various techniques and measures that are specifically intended to describe, visualize, and summarize data. Usually used when dealing with large datasets, these techniques define the **descriptive** statistics.

In the following a brief explanation of the measures used in this work will be provided:

- **Mean Value:** refers to the average of a set of values. It is calculated by adding all the values in a set and then dividing the sum by the number of values.

- **Median Value:** is the middle value in a sorted list of numbers. If the list has an odd number of elements, the median is the middle one. If the list has an even number of elements, the median is the average of the two middle values.
- **Mode:** is the value that appears most frequently in a set of data. A set of data may have one mode, more than one mode, or no mode at all.
- **Range:** is the difference between the largest and smallest values in a set of data.
- **Variance:** is a measure of how spread out a set of values is. It is calculated as the average of the squared differences of each values from the mean.
- **Standard Deviation (STD):** is another measure of values distribution. It is calculated as the square root of the variance.

2.2.9 F-test

The F-test is a statistical test that is used to compare STD or variances between two (or more) groups of samples. It is based on the assumption that the input data follows the probability distribution known as F-distribution (that also gives name to the test). As per other statistical tests, the F-test produces an F-statistic and a p-value. The F-statistic measures the ratio of the variance between groups to the variance within groups, while the p-value indicates the statistical significance of the results obtained. A large F-statistic represent a great variance between groups and a relatively smaller variance within each group. A p-value below 0.05 (a common threshold value) signifies a sufficient statistical significance of the test, while a value higher implies that the outcome of the test may be a coincidence.

This statistical tool is typically used in two applications, briefly explained in the following:

1. **Analysis of Variance (ANOVA):** in this case the means of three or more groups are compared, to determine if statistical differences are present between groups. The null hypothesis (H_0) infers that all group means are equal, while the alternative hypothesis (H_a) implies that one or more means are different by some amount.

2. Variance Comparison: This F-test is used to compare the variances of two independent samples to determine if they are significantly different. This test is typically used to assess and compare the consistency between two variables.

2.2.10 Granger's Causality

Granger causality is a statistical concept and method used to determine whether one time series can help predict another time series. It is widely used in various fields, including economics, finance, and the natural sciences, to explore causal relationships between time-dependent data. The theory behind this concept revolves around some key components and assumptions:

- Input data must be in the form of a timeseries, which consists of a sequence of observations collected at equally spaced time intervals.
- Past values of a variable X can provide information to estimate future values of a variable Y. This statistical concept exploits the analysis of lagged values of the variable X to determine if those can help the determination of accurate future values of another variable Y.
- Granger's causality can provide information and measure about causation only in the prospective of "influence": it is not intended to determine physical, philosophical, or deterministic cause-effect relationship. It can although be used in this perspective if paired with other relationship measures.

This statistical causality measure is performed with hypothesis testing, by comparing two estimation models of the future values of the variable Y:

- The first model is autoregressive and predicts future Y values using as input only its past values.
- The second model differs from the first for the addition of the past values of the X variable as input data.

Given that the null hypothesis (H_0) is that X does not Granger cause Y, meaning that the second model does not significantly improve the results of the first model, a statistical test is performed. Usually, the H_0 is tested with F-test or chi-squared test.

If the result of these test, in terms of F or chi-squared statistics and p-values, reject the null hypothesis, an influence of X in the values of Y can be confirmed.

2.2.11 Coherence

Signal coherence refers to the degree of similarity or consistency between two or more signals in terms of their phase and frequency relationships. In other words, it measures how well signals maintain a constant phase relationship over time and how their frequencies are related. Coherent signals have a fixed phase difference, and their frequencies are related in a consistent manner, while incoherent signals exhibit random phase variations and may not have a stable frequency relationship.

3 Materials and Methods

This section will cover the main workflow that has been followed in the analysis of the available data, as well as a brief summary of the acquisition process and the previous study from where the idea of this research has originated.

3.1 Dataset Acquisition

Data has been acquired during the study conducted by Marco Strada and Ruggero Cattaneo²⁴. Their study aimed to take up, making use of the latest technology in the field of sensor imaging and computer science, the work done by Frymann in 1971. In fact, despite the growing interest in the field of cranial osteopathy, no other objective measurement studies of cranial rhythmic motility have been carried out since that first approach made more than 50 years ago, aside from the work of Rasmussen et al. in 2021. The authors therefore set out to find a way to measure CRI rhythm with the goal, which is also in common with this work, of finding an objective and repeatable measurement of this rhythm, thus proving its existence in a scientific way.

Several signals were acquired in the recording sessions:

1. Blood Volume Pulse, via a PPG sensor placed on the fingertip of the third finger of the right hand.
2. Body temperature, via a probe thermometer inserted inside the PPG band.
3. Skin Conductance, via two electrodes placed on the fourth and second finger of the right hand.
4. CRI, via a band with tensiometer placed around the skull.
5. Respiration, via a band with tensiometer placed around the chest at the level of the last ribs.
6. EMG, via bipolar electrode at the level of the right suprahyoid musculature.
7. ECG, via three electrodes (right and left shoulder, as well as under umbilical area)

Unfortunately, only some of these data has been available to analyze in this work: the BVP, IBI, Respiration and CRI signals, as well as the HRV, extrapolated from BVP.

CRI and Respiration signal have been acquired with a sampling rate of 256 Hz, while the BVP signal has a sampling rate of 2048 Hz.

Data acquisition was performed under conditions that were as stationary as possible for all subjects. The recording sessions, lasting from 6 to 55 minutes, were carried out during the morning, asking subjects to have only a small breakfast before the acquisitions. Five subjects in particular were asked to sustain a few brief moments of apnea during the sessions, to assess any change in the CRI signal under this condition.

3.2 Dataset Import

The available dataset consists of the collection of the above-mentioned signals for each of the 39 patients who formed the study group in the previous work.

The data were stored in .txt format in several folders, one for each patient. It was therefore necessary to create an initial MATLAB code, which will be analyzed below, suitable for importing the data and converting them into a format useful for subsequent processing.

To make the work as generalized as possible, the very first step was to make a function capable of determining the operating system in which the code is executed, returning as output the number of hidden items in the directories and the correct direction of the slash needed to indicate file paths. In fact, there is a difference between Unix-based systems (Mac OS and Linux) and MS DOS-based systems (Windows) concerning these two parameters. In fact, Unix and DOS systems use “/” and “\” respectively as hierarchical pointers in the description of file paths. In Unix systems there is also one more hidden element at the beginning of each directory than in MS DOS systems (namely 5 instead of 4). The algorithm then proceeds with the extraction of patient names by scanning the root directory containing the dataset.

The next step involves the actual import of the data, to convert them into MATLAB variables that can then be used for further analysis. We proceed to import the individual .txt files each containing the raw data concerning a particular signal, represented with a sample for each line. The only exception are the CRI and respiration signals, which are stored together in a single file on two columns.

The process of converting the latter two signals required special attention because, probably due to oversights at the time of acquisition, the order of the two signals in the respective columns of the .txt file is not always the same: most files have the breath signal in the first column and the CRI signal in the second, but in some patients the data are reversed. With the information found from the previous study, it was possible to determine that the mean value of the raw CRI signal is significantly higher than that of the abdominal band signal. Therefore, an additional step was implemented in which the mean of each of the signals is calculated: the signal in the column with the higher mean is then imported as "CRI" and the other as "RESP".

The data are then imported and saved in a MATLAB struct named "Data", which is organized hierarchically with substructures having a progressive index of the form "P1, P2, ..." as their name. The order of the patients is not changed during import, so the sequence name given above is consistent with the index of patient names extracted at the beginning by scanning the main dataset directory.

An identical process to that just described is carried out to import data on the five patients who sustained brief moments of apnea during the recording sessions. Their data was stored initially in a separate struct named "Data_Apnea", but subsequent considerations made during the development of the main analysis pipeline have pointed out that it was more convenient to have all the data in one MATLAB struct. In the final version of the import code, data for patients who sustained moments of apnea are then saved at the tail end of the struct containing data of the other patients.

A final step related to the creation of the dataset in MATLAB format was to remove, after confirming its lack of validity, the 10 seconds at the extremes of each record. In fact, looking at the complete signals, it was noticeable that these initial and final portions were still residual from the moment of sensor setup and the moment when the subjects stood up at the end of the recording.

The data imported and organized as described above were then saved in a .mat package containing the main struct ("Data"), the index of patient names, and the progressive identification index used within the struct. The latter is saved since it is needed later to iterate over the main struct in the analysis of multiple patients.

In the following page a summary diagram of the MATLAB dataset creation process is presented (Figure 7). The creation of a script suitable for importing the data and storing it in native MATLAB format, although time-consuming to design and implement, proved to be an efficient step from the point of view of the computational time required for the overall processing of the analysis. The time required by the computer to run the data import script code is in fact 39.2 seconds, time that would have been required to wait for each run of the main script if it had not been unbundled. This choice thus allowed the dataset to be imported from file only once (since the code reached its final version). In the many runs of the main code, it was then only necessary to load the .mat file containing the dataset, with an average loading time of 4,4 s.

Dataset loading time	From .txt file	From .mat file	Improvement
	39,2 s	4,4 s	8,9 x faster

Table 2: Dataset loading performances.

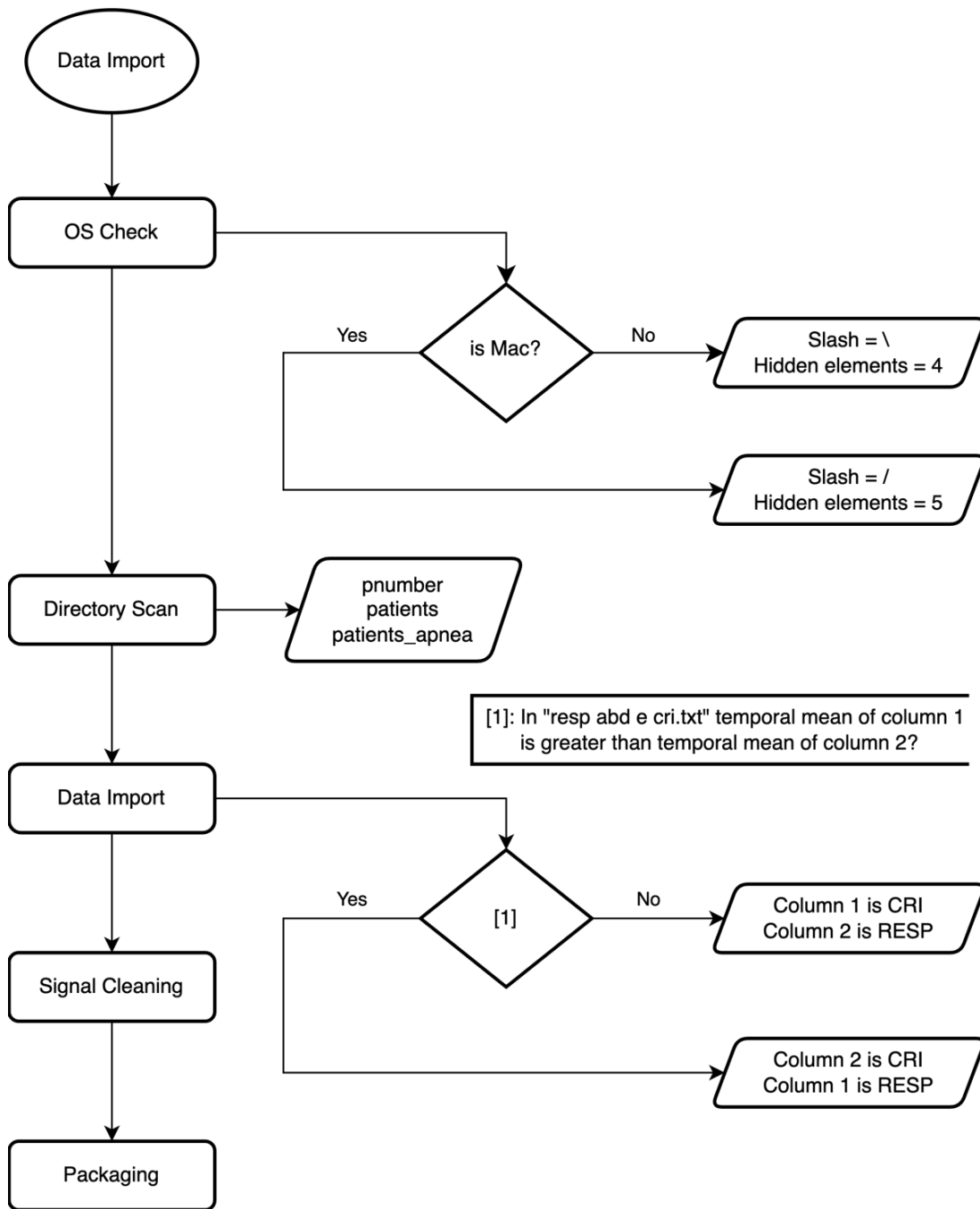


Figure 7 Diagram of Data Import code

3.3 Analysis

In the following section an in-depth description of the main analysis code will be provided. The work is structured in multiple blocks that are as independent as possible. When possible and convenient some parts of the code have been further generalized and hived off from the main code, making them MATLAB functions.

3.3.1 Interpolation of HRV

The first action in data analysis was to extrapolate the peaks related to the systolic pressure wave from the BVP signal in order to derive the time distances between successive heartbeats. In fact, the temporal data for this information, denoted IBI (Inter Beat Interval), was already present in the dataset, but it has been chosen to derive it from the BVP signal to have a double check on the IBI data.

This was done in various steps:

1. Calculating the time difference between each two consecutive peaks in the BVP signal.
2. Assigning the obtained value to a specific point in the BVP time vector, chosen to be the mean instant between the two peaks.
3. Interpolating these points in the main time vector.

The information obtained in the steps 1 and 2 had to be interpolated in order to have an HRV signal with the same temporal resolution as the others, basic requirement to the further analysis passages.

In some patients, interpolation led to some *Nan* (Not a Number) values among the first and last seconds of the track. Since the number of *Nan* points was far below 1% of the total samples, it has been chosen to replace these points with a random value within the STD of the signal.

In this section of the code, the BVP signal has also been resampled to 256 Hz, to match the sampling rate of the other signals. Also, given that the area of interest of this research is focused on the low and very-low frequencies, there is no particular purpose in having a signal sampled at a high frequency.

3.3.2 BP Filtering

The analysis process then continued with signal filtering. In this regard, several filtering techniques were examined, to determine the most appropriate for the work. The choice fell on different high-order FIR filters, implemented with double pass to achieve zero-lag filtering.

The advantages of this filtering technique included the quality of signal reconstruction, computational performance, and versatility in choosing the frequency bands to be filtered. The architecture of FIR filters guaranteed linear phase.

It was chosen at this point in the work to analyze three different frequency bands separately on each signal:

- Medium Band (M), from 0.4 to 4 Hz.
- Low Band (L), from 0.05 to 0.5 Hz.
- Very Low Band (VL), from 0.0017 to 0.05 Hz.

Respectively, these bands represent the following cycles per minute (cpm):

- M Band, from 24 to 240 cpm.
- L Band, from 3 to 30 cpm.
- VL Band, from 0.1 to 3 cpm.

The division into the three bands listed above was done in order to determine more precisely whether any correlation with other signals was located in a specific frequency range. The three bands, particularly the M-band, are quite large when considered from a cpm

perspective, but unfortunately given the large discrepancy found in the literature, it was not possible at this point in the work to select the frequencies more narrowly.

Before filtering operations, the signals have been then downsampled to 8 Hz, since the useful frequency ranges were well below the 128 Hz threshold for which there would have been reasons to maintain the original 256 Hz sampling.

For each signal it comes to this point to have different versions:

Signal	Sampling Frequency (Hz)	Bandwidth (Hz)
Original	256	0 - 256
Downsampled M-Band	8	0.1 - 4
Downsampled L-Band	8	0.05 - 0.5
Downsampled VL-Band	8	0.0017 - 0.05

Table 3: Different versions of the signals obtained downstream of filtering and downsampling.

3.3.3 PSD

In these initial stages of analysis, designed to determine as many characteristics as possible regarding the signals, a step of great importance is definitely the calculation of the power density spectrum (PSD). Since it has been assumed that during the writing of the code there might be a possible need to change parameters regarding the PSD, a function was implemented that would be able to determine them automatically.

The automated calculation of these parameters was based on two inputs: the sampling rate and the required resolution (in terms of frequency).

The basic structure of the function determines an initial estimate of NFFT, the number of points to be considered for the FFT, by dividing the sampling rate by the required resolution. The function then iteratively searches for the power of 2 closest to the previously estimated value for NFFT, as using powers of 2 increases performance.

This search is done by calculating from cycle to cycle the difference between the NFFT estimated with the input data and the i -th power of 2 and verifying that this difference is less than the one calculated at the previous iteration. For each cycle, the value of “ i ” is increased. The cycle is stopped when the difference in the previous cycle is less than that calculated in the active cycle. The actual value of NFFT then turns out to be that of the penultimate cycle executed. The function then also proceeded to determine the window and overlap parameters as one-fourth and one-eighth of the value of NFFT, respectively.

The PSD calculation is then carried out for the nine (three for each band) signals from each of the 37 subjects selected in the database. From the values obtained, averages (over frequencies) are then extrapolated for each of the signals.

Having completed the tasks to better define the characteristics associated with the signals, a second phase was conducted in which any correlations between the signals were sought to be understood.

3.3.4 PLV

The first correlation measure that has been implemented concerns the phase of the signals, and in particular the correlation between the phase of the CRI signal with that of the other three signals: namely, the PLV. This measure was also obtained using a dedicated function, again with a view to generalizing and streamlining the main script.

This function consists of four main steps:

- Computation of the Hilbert transform per each signal.
- Extraction of the phase information from the analytical signals.
- Calculation of the relative phase by subtracting phase values between the two signals.
- Averaging of differential phase.

Again, in the case of this metric, statistical measures were then calculated to give an easier and more immediate interpretation of the data. The mean value and STD of the PLV was calculated for each patient.

3.3.5 Coherence

To obtain further information regarding the possible correlation between the signals, the measure of coherence between them was also calculated. Specifically, this metric was calculated between the CRI signal and the others in the dataset (breath, BVP and HRV).

The coherence calculation was performed for each of the three bands into which the signals were previously divided. The *mscohere* function was used, which calculates coherence as the ratio of the cross-power density spectrum to the product between the auto power density spectra of the two signals given as input.

To visualize the results, a composite plot was made with the different frequency-averaged coherence measures for each of the bands into which the signals were divided.

In accordance with what was seen during the literature search done in the preliminary stages of this study, within the complex waveform of the trace related to the CRI phenomenon it was expected to find long oscillations, as suggested by the findings of several osteopaths over time.

The next three sections go on to describe in detail the part of the code related to finding these oscillations and their possible correlation with similar waveforms in other signals contained in the dataset.

Attention has further been drawn to this part of the analysis because it was noticed during the many signal observations that on several occasions the presence of an abnormality in the exhalation phase corresponded to a spike in the CRI signal. This led to the suspicion that there might be a non-random but functional correlation between these two phenomena.

3.3.6 Peak Detection on CRI signal

The first approach by which the alleged cranial oscillations were tried to be investigated was carried out through the analysis of peaks in the CRI signal. A specific MATLAB function was implemented for this purpose, with the aim of streamlining the main code and making it possible to easily extend the work in case it is taken up with other available signals in the future.

The analysis focused on two signals in particular, as will be better explained below, namely the CRI signal and the breath signal, as they appeared to be the most visually and physiologically related.

This analysis, although written from the code point of view in the most generalized way possible, was conducted with the intent to see if there was a particular morphological level match on the breath signal in the windows identified on the peaks of the CRI signal.

3.3.6.1 External Function

In fact, the function takes two signals as input, and computes the peak calculation on the first one, while showing the relative temporal position on the second signal as well, in order to highlight possible correlations. The function also incorporates an extrapolation of random data from the two signals, for subsequent validation operations. Other parameters, necessary for the proper operation of this secondary code, are also requested as input, as will be explained below.

As a first step in the aforementioned function, the search for peaks in the first input signal, in this case the CRI, is performed with the MATLAB function “*findpeaks*”. The parameters for the peak search have not been made explicit as input to the function, but rather fixed after extensive tuning based on the trial and error done on the dataset at hand. In any case, they remain obviously editable by opening the function. The parameters chosen for the *findpeaks* function are:

- Minimum Peak Height of 15% of the standard deviation of signal 1.
- Minimum Peak Distance of 1 second (8 samples, given the 8 Hz sampling rate).
- Minimum Peak Prominence of 50% of the standard deviation of signal 1.

At this point, it has been obtained as output from the peak search a vector containing the time instants at which these peaks were detected. The data about the length of this vector is used to extrapolate, again from the first signal given as input, a series of equal lengths of random points.

Both vectors, the one for the peaks and the one with random data, are subjected to a verification process: in fact, it is checked that it is possible to extract a window of signal (whose extension from the central point is one of the inputs) centered on the peak without exceeding the limits of the signal. As an example, consider a peak detected on sample number 130 and a length relative to the window extension of 300 samples. The total length of the window would be 601 points (twice its extension plus the center point), but the initial point should be found 170 instants before the signal actually begins.

This problem is obviated by removing peak and random points that are at a distance from the beginning or end of the signal less than three times the window extent. This control, which is rather conservative, also aims to eliminate any spikes resulting from noise in the initial and final instants of observation.

The removal of these points, since they are identified with their position within the vectors, was done by analyzing the vector from the end toward the beginning, since the removal of a particular point results in the shifting of all downstream indices.

The structure of the function continues with a few steps necessary for the proper display of a double plot containing markers that identify peaks on both signal 1 (on which they were calculated) and signal 2, overlaying the signal tracks. The output of the previously mentioned figures (one for each subject) is dependent on an input variable (of value 0 or 1) that enables or disables this graphical output.

The final part of the function saves within three matrices (outputs of the function, along with the time index of the peaks) the following data:

- Windows of signal 1 centered on its detected peaks.
- Windows of signal 2 centered on signal 1 peaks.
- Windows of signal 2 centered on random points.

The function is placed in the main script within a for loop that iterates over the number of subjects in the dataset. Outputs from the function are saved in variables within the respective substructures related to the individual subjects.

3.3.6.2 Clustering

3.3.6.2.1 Whole Dataset

The second step related to the search for peaks involves their classification by clustering. A first iterative cycle unifies the vectors related to the windows acquired in the previous phase, extracting them from the substructures of each subject. Three cumulative matrices are then obtained, respectively containing the CRI signal windows centered on its peaks, respiration signal windows on the corresponding temporal portions of the CRI ones, and finally the randomly selected windows, also on the breath signal.

Clustering is then done on the matrix related to the breath windows centered on the CRI peaks, using the *kmeans* function. Two parameters of the function have been specified:

- Distance: the *correlation* method has been chosen since the breath waveforms have widely varying amplitudes, and this method involves normalization of the data before clustering.
- Start: *cluster* mode was chosen, which performs preliminary clustering using 10% of the data to determine the initial clusters and their centroids. it was noted that through several attempts this method yielded the most consistent results.

Clustering results have then been presented on different plots. Since the number of clusters was changed frequently in the development stages, a system for automatic subplot rearrangement has been implemented. Given that they are organized into rows and columns, these were defined as:

- Rows: value rounded to the lower integer of the square root of the number of clusters.
- Columns: value rounded up to the next higher integer of the square root of the number of clusters.

As for the progressive index, the cluster one was used. In this way, by iteratively cycling over the total number of windows acquired, each was plotted in the correct subplot. Since the clusters were formed based on data from the breath windows, more care was taken in making the graph related to them. An average curve representing the cluster was also computed, so that it could be inserted as an overlay to the raw result. A similar process was performed for randomly centered window data.

As an additional statistic, information on the population quantity of the various clusters was also calculated so that its validity could be more accurately assessed.

3.3.6.2.2 Selected Data

At a later stage, the clustering process was enriched with an additional step. From the results for other numerical analyses, as well as additional visual consideration, several subjects were selected, whose acquisitions seemed most promising in terms of quality and significance.

To better understand whether the results of the spike search and clustering were biased by unreliable signals from some subjects, a separate clustering was performed on the signal windows for these selected subjects. The methods will not be explained in detail since they are the same as those implemented previously for clustering operations related to the whole dataset. Again, both peak-related and random windows were selected.

All the processes listed in Section 3.3.6 were repeated on all three signal bands.

3.3.7 Anomaly Detection on RESP signal

Further investigation has been attempted regarding the possible correlation between breath and CRI signal. This section will detail the process in which possible abnormalities in the breath signal were searched for, aiming to find a possible correlation of CRI with these.

3.3.7.1 Local Minima Detection

Since the anomalies noted on the breath signal presented a rather repetitive pattern, with a slight peak in the exhalation phase, where one would expect a monotonic decreasing pattern, it was chosen to investigate the latter phenomenon.

Local minima of the breath curve were then sought, defining the minimum prominence of these peaks as a parameter of the *islocalmin* function, so as to exclude the smallest variations given by interference or background noise. The value chosen for the minimum prominence was 0.01. Having found the local minima and their prominence, the peaks with a prominence value less than 15% of the mean value were selected. This step was done to exclude local minima related to normal breath fluctuations, which have significantly greater prominence and were not of interest for this the analysis.

In summary, through the minimum prominence parameter of the *islocalmin* function and this last selection step, it was possible to obtain two vectors (one logical and one of values) related to peaks with prominence between 0.01 and 15% of the average value of it.

At this point, the two maximum time intervals between successive local minima were calculated. In addition, temporal markers related to the beginning and end of these two signal sections were also extrapolated. This was done because it was necessary for the continuation of the analysis, as will be detailed in the next subsection.

A matrix is also populated at this point with temporal information about the peaks.

3.3.7.2 AI Anomaly Detection

Since the visually noticed abnormality on the breathing signal did not have a perfectly equal repetition, it was thought that a plausible tool to look for different variations of it could be an artificial intelligence algorithm, as it could adapt to the changing characteristics of these abnormalities.

From a search done to figure out what kind of algorithm was most appropriate to use, a recently implemented MATLAB object (introduced in version R2023a) called *DeepSignalAnomalyDetector* was found. This package implements an autoencoder type architecture that can detect anomalies in different types of signals. There are no particular limits on the length of the anomalies, from being almost instantaneous to the entirety of the signal.

Being an autoencoder architecture, this network is able to reconstruct the signal from an input given as a training signal. Once the signal is reconstructed, portions of the original signal that deviate from the reconstructed signal by a value greater than an a priori chosen threshold are reported as anomalies. The information extracted earlier regarding the length of the signal portions without small local minima has been used at this point. Before starting the network learning process, it has been made possible for the user to decide which of the two longest sequences of "normal" signal to use as a reference for network training.

At this point, the portion of the signal to be used as the test set is automatically defined as the whole signal.

Below are the parameters used by the convolution and deconvolution algorithm:

- Filter size = 128.
- Number of filters = 8.
- Number of downsample layers = 4.
- Threshold method has been set to "contaminationFraction", which calculates threshold automatically.

- Training has been done with 200 epochs.
- Adam optimizer has been used.

This model is the result of parameters optimization done through several attempts. Two other models have proven to be quite good, although not performing as well as the one described above. Below is a table with the parameters of the three models summarized:

Model	Filter Size	N. of filters	N. of DL	Threshold method
Current	128	8	4	<i>contaminationfraction</i>
Second	64	32	8	<i>contaminationfraction</i>
First	64	16	6	<i>contaminationfraction</i>

Table 4 AnomalyDetector models

As can be seen from the table above, the current model is the simplest of those displayed. Indeed, it was concluded that for this type of anomaly detection, a simpler model but with a larger filter size would give higher and more consistent performance.

The last step in this portion of the analysis was to graph the results obtained. To do this, the *deepsignalanomalydetector* object provides some dedicated functions, but these were not exactly suited to the purpose required here. The main results visualization tool in fact makes a composite graph in which the original signal, the reconstructed signal and the anomalies found are displayed, superimposed on the original signal. Since this was not the main information to be obtained from the analysis, other plots were made.

Unfortunately, no information on how to extract the calculated information is provided in the documentation for this object. It was therefore necessary to extract it manually from the graphical plot data provided by the object. After some trial and error, it was possible to extract from the graphical data the information about the portions of the signal identified as anomalies so that they could be inserted as an overlay to the CRI signal.

3.3.8 Granger's Causality Analysis

One of the last steps of analysis in this work was the calculation of causality according to Granger. To carry this out, the **Granger Causal Connectivity Analysis**²⁵ toolbox was used, which provided a good foundation of tools to develop this part of the code. The code provided as a demo of the toolbox functionality was used as the basis for the development of what was later implemented as an external function for calculating Granger causality. The process is divided into two main steps: the calculation of causality in the time domain and then in the frequency domain.

For the development of the code, the track given by the manual attached to the toolbox was followed.

Input data (CRI, BVP, breath, HRV) are organized into a single matrix. It is suggested by the manual to apply some data pre-processing steps, which are redundant in this case, since the data have already been processed previously. Of these steps, therefore, only those not performed earlier in the code have been included, namely:

- Normalization
- Calculation of the derivative

The next step is to verify the stationarity of the signals from the point of view of covariance, through the ADF and KPSS tests. The derivation step, mentioned earlier, was added later to ensure the positivity of the two covariance tests (as suggested by the guide), which initially yielded negative results.

The necessary steps were then taken for the actual calculation of causality according to Granger. The toolbox also provides the functions needed to visualize the data, both in the time and frequency domains. The guide provided with the package was also followed with regard to these steps.

Given the complexity of the analysis in question, during development this was initially implemented for a single patient, with the idea of later expanding it to the entire dataset. This last step should have been accomplished by taking advantage of the toolbox's ability to work with multi-trial data, but unfortunately during the development of this part of the code, problems were encountered with some of the toolbox's internal files. After several modifications to the toolbox functions some problems were solved, but unfortunately a particular corrupted .MEX file prevented the creation of a working function to analyze the dataset in its entirety as a multi-trial event.

3.3.9 Spectral Subtraction

The last analysis step implemented in this work was spectral subtraction. This was implemented since the previous steps did not provide very satisfactory results, so the question was raised at this point whether it was worthwhile to try to further improve the quality of the signals within the dataset.

The spectral subtraction methods by Berouti and Boll were used, implemented with the help of two functions available on the MATLAB Exchange portal^{26,27}. Again, the two techniques were applied separately for signals in the respective frequency bands.

4 Results

The main objective of this research was to characterize and explore the possible connections of the CRI signal with other biological signals. A review of the literature on the topic, the theoretical background concerning the research, and the methodologies used during the analysis process were described in detail in the previous chapters. In this chapter, the results obtained will be presented.

4.1 Visualization of Signals

A non-negligible portion of time in this work was devoted to a preliminary observation and understanding of the signals included in the dataset. In Figure 8 it is possible to observe how the set of signals related to subject P10, chosen as an example. The signals displayed in this graph have not yet been processed in any way, except for the interpolation of the HRV signal, as explained in Section 3.3.1.

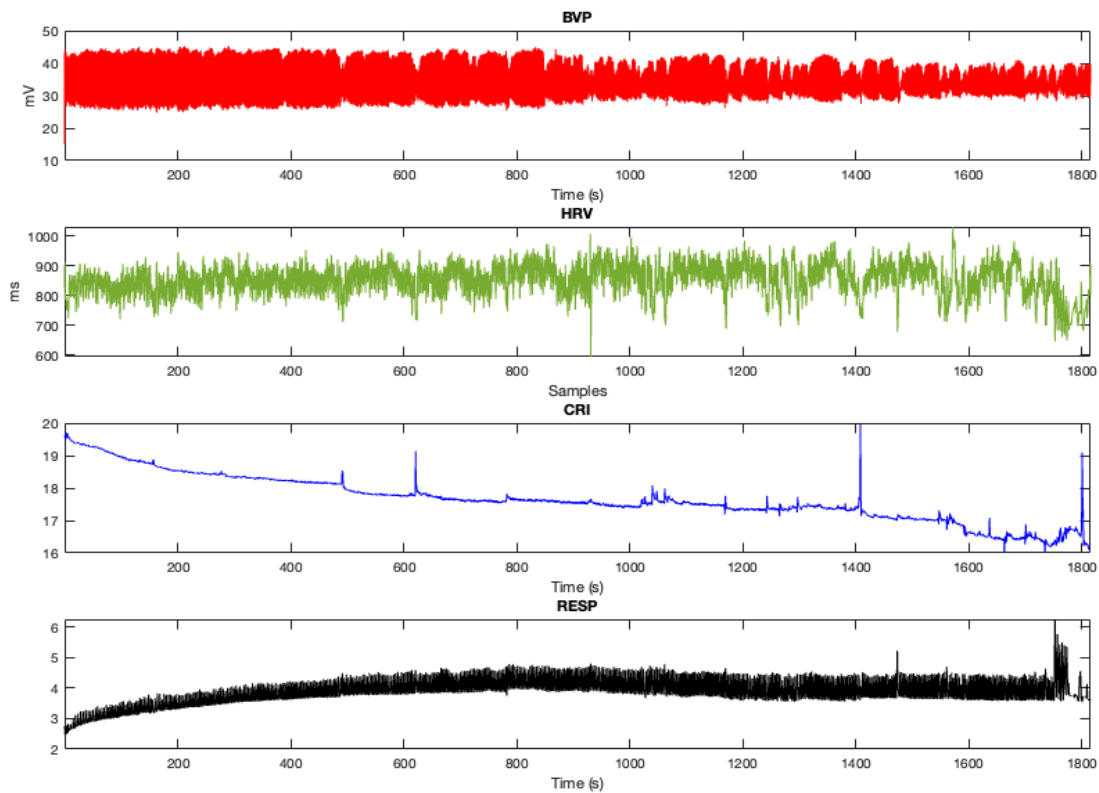


Figure 8 RAW Data Plot

The signals, from a first overall view, have substantially different morphologies from each other. Looking more closely, however, one can denote distinctly similar behaviors, as shown in Figure 9, where the time scale has been reduced to 10 seconds.

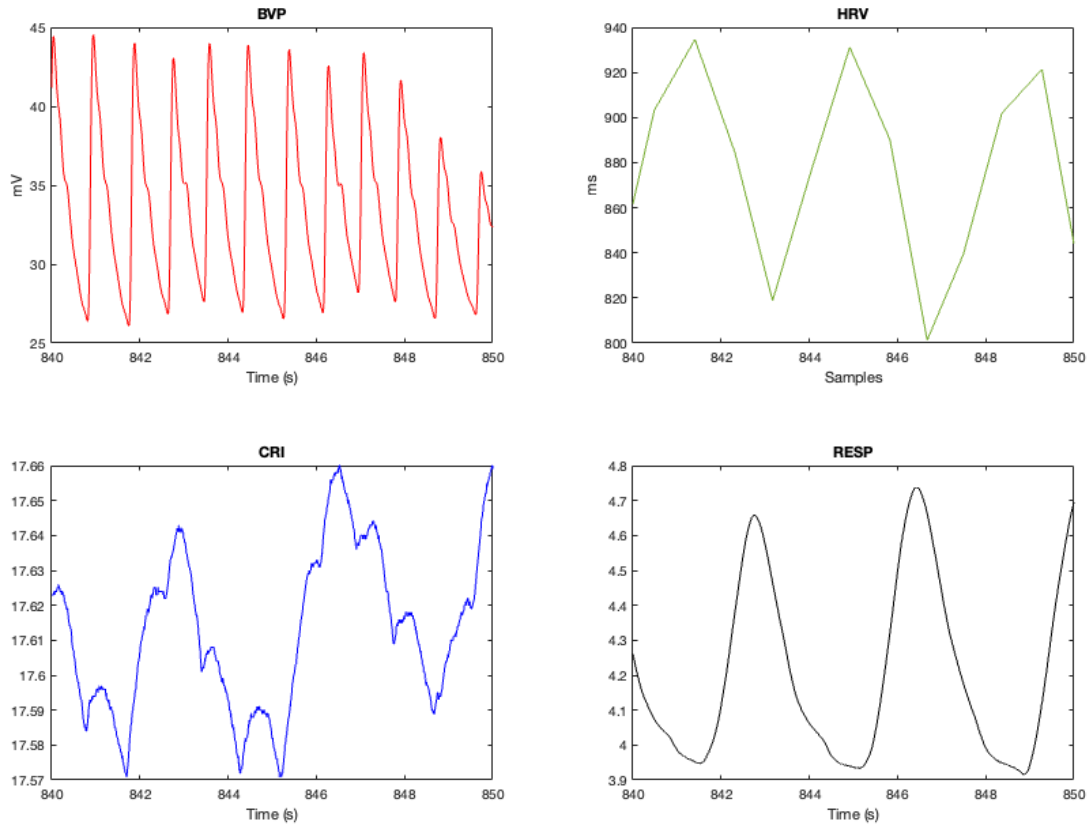


Figure 9 Temporal detail of signals

Indeed, it can be seen in this detailed view how all the signals exhibit a fundamentally wave-like pattern, but with clear differences in frequency. In fact, already from this view it is possible to appreciate the similarity between the CRI signal and the breath signal.

Another characteristic trend, already highlighted in Figure 1, is that of the BVP signal, which presents a more pronounced peak corresponding to ventricular contraction and another less prominent one. Local minima, on the other hand, are related to the diastolic phase.

4.2 Filtering

Aware of the indications provided by the literature review regarding the palpation frequencies of the CRI signal in cycles per minute, the signals were filtered, creating three copies of each. Each of the copies of the signals was filtered at a different frequency band, as already specified in Section 3.3.2. Below are the bands chosen:

- Medium Band: from 24 to 240 cpm.
- Low Band: from 3 to 30 cpm.
- Very Low Band: from 0.1 to 3 cpm.

Figure 10 shows the overall and a detail of the filtering performed on the CRI signal.

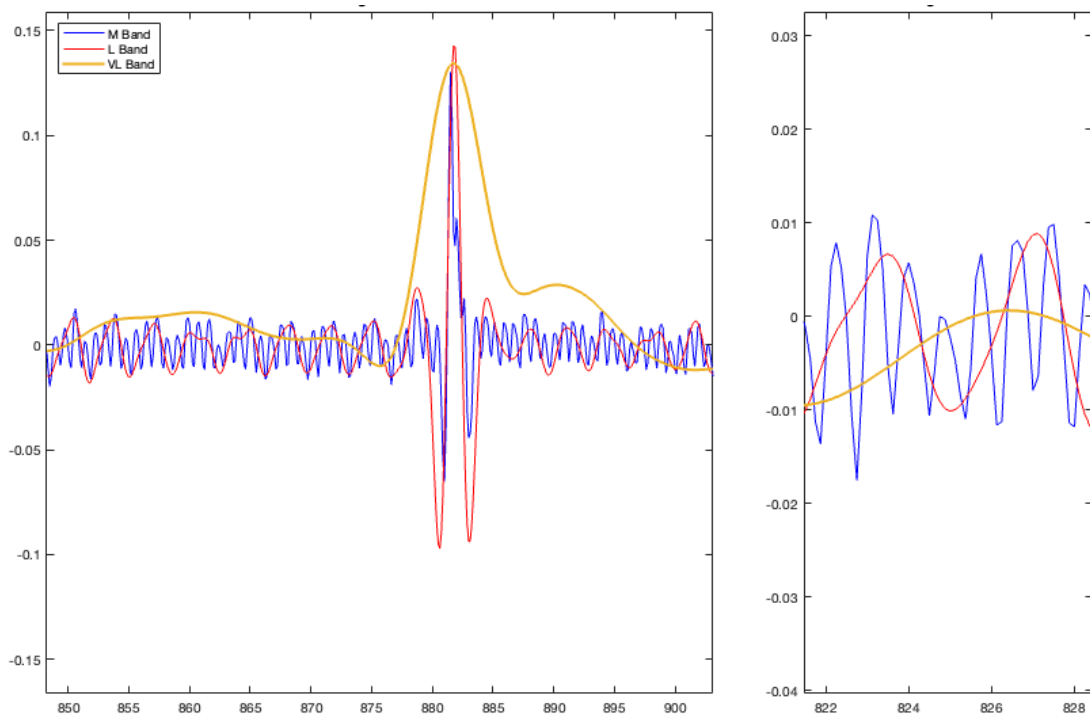


Figure 10 Overall and a detail of filtered CRI signal

In the figure, as shown in the legend, the M-band filtered CRI signal can be seen in blue, the L-band signal in red, and the VL-band signal in yellow. The choice of dividing the signal into

three bands proved to be correct, as subsequent analysis showed different results on the different bands, which otherwise could not have been seen.

As early as this stage of the analysis, it is already possible to appreciate, particularly from the graph on the right in Figure 10 and from Figure 9, how the different components of the CRI signal can already be visibly associated with the remaining signals: the similarity between the M-band and the BVP signal is particularly evident, as is that of the respiration signal with the L-band.

4.3 PSD

Following the filtering operations, analysis of the signals from a frequency domain perspective was begun. The results of the PSDs calculated on the various versions of the signals have been summarized in three graphs in Figure 11, Figure 12 and Figure 13, which show the power spectra of the signals in the Medium, Low and Very Low bands, respectively.

4.3.1 M-Band

Looking at the M-band PSD, it was immediately apparent that most of the power of the BVP signal was concentrated above 0.5 Hz. This finding is expected since that signal describes the blood pressure wave, which is dependent on heart rate. This usually varies between 50-70 cycles per minute in healthy subjects at rest, giving explanation for the peak located at 0.93 Hz.

In addition, the double-peaked nature of the BVP signal (see Figure 1) is also evident when looking at the area related to the 1.7-2.7 Hz range, where another peak, albeit smaller than the previous one, is noticeable.

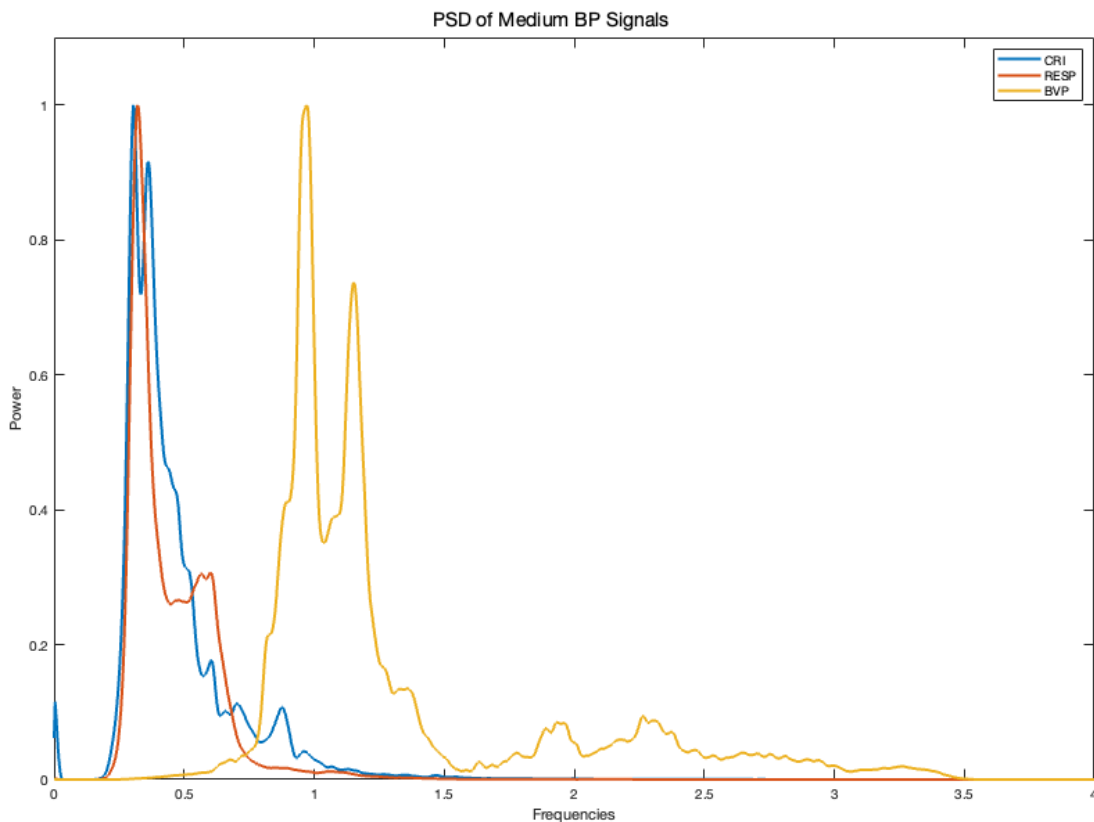


Figure 11 PSD of M-Band signals

4.3.2 L-Band

This frequency range (from 0.05 to 0.5 Hz), also gives room for some interesting observations, as can be seen in Figure 12. Indeed, it can be clearly seen that both the breath and the CRI signal have a peak on 0.3 Hz. The curves descending from this peak does not have high steepness, going to delineate an area between successive local minima of about 0.2 Hz. This area goes to cover the typical values of the resting breath rate, corresponding to about 12-18 cycles per minute.

Adding to this phenomenon is also the presence of some CRI signal peaks (in blue) at about 0.22, 0.24 and 0.36 Hz.

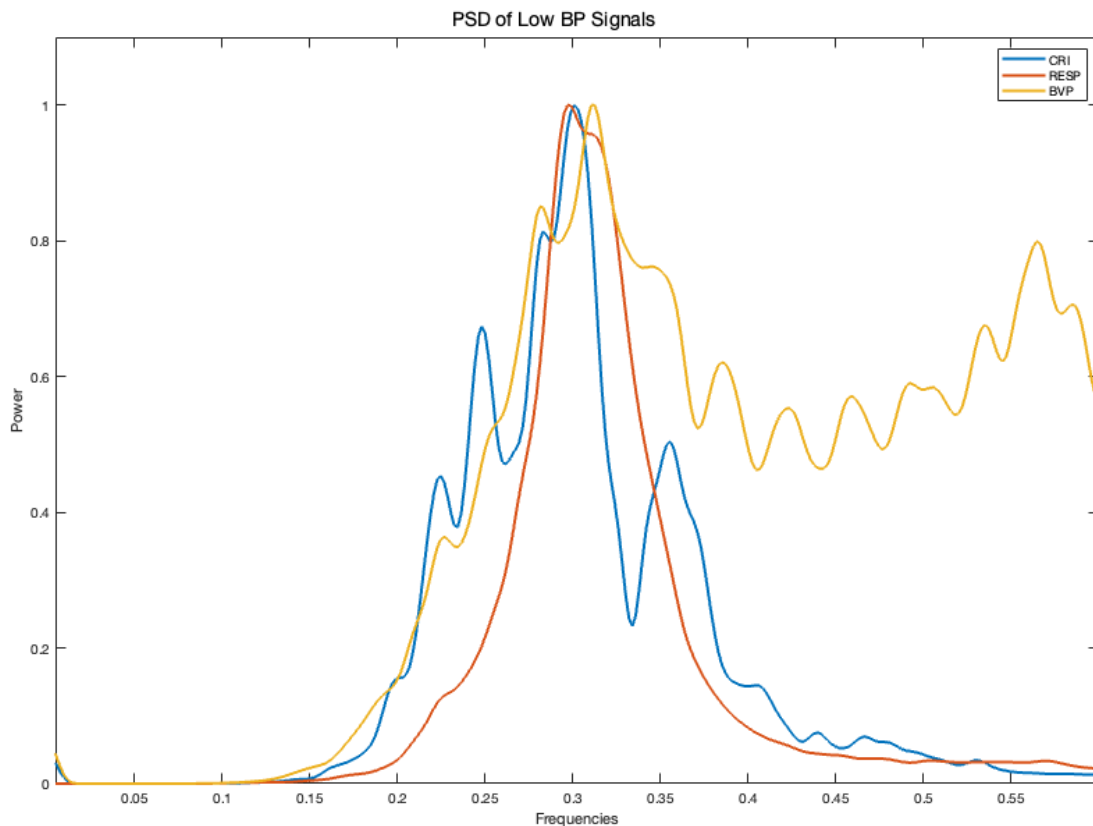


Figure 12 PSD of L-Band signals

4.3.3 VL-Band

Looking at Figure 13, displaying the very low band of the signals, it is immediately possible to see that the frequency contents of respiration, BVP and CRI are not identical. CRI signal present a peak at 0.087 Hz, while the respiration signal shows activity at 0.11 and 0.13 Hz. The BVP signal on the contrary, has a broader frequency content, enclosed in the range of 0.04 to 0.16 Hz, where the other signals appear to have lower power contributes.

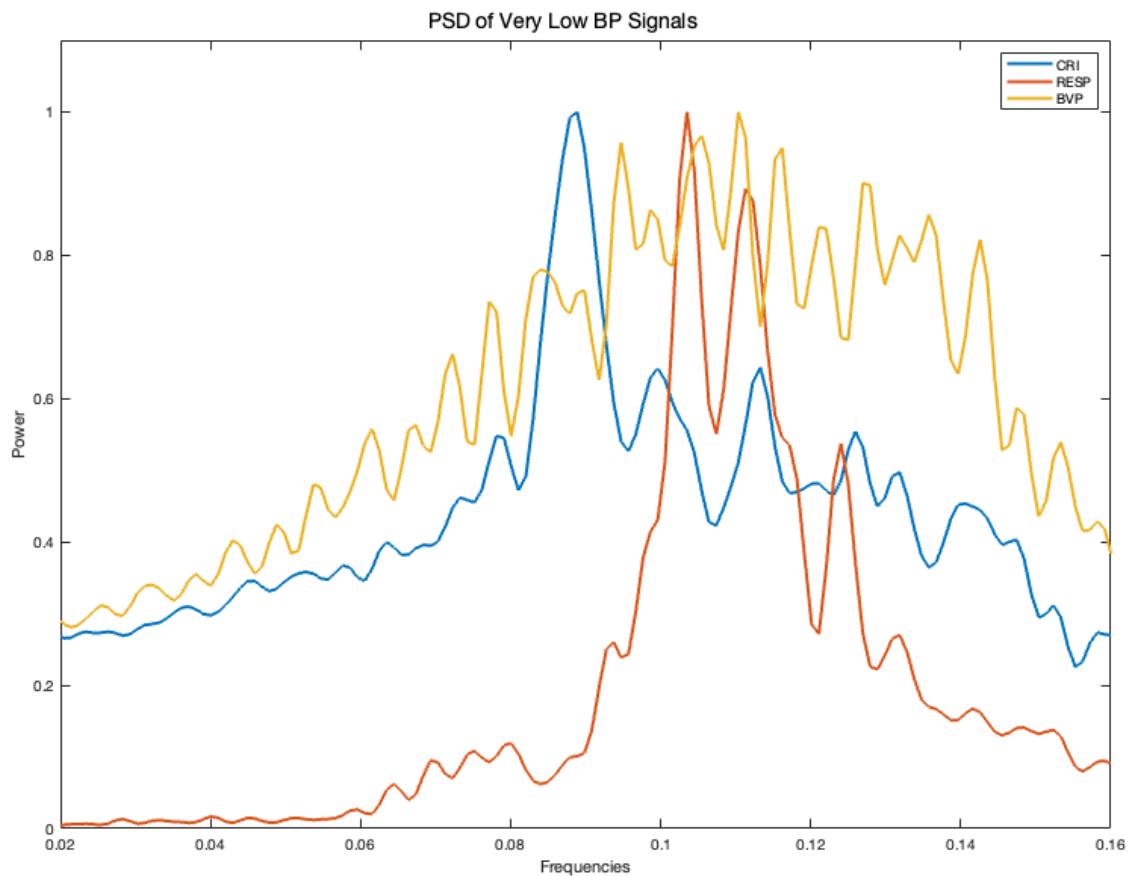


Figure 13 PSD of VL-Band signals

4.4 PLV

Several signal similarity measures are now presented. The first one introduced here is that of PLV, Phase Locking Value. This measure indicates the degree of correlation of two signals by going to calculate the phase difference between the two at each instant within a given time window. An averaging operation is then performed on the window. The process is then

repeated by translating the window to cover the entire length of the signal. In Figure 14 and 15, it is possible to appreciate by bar graphs the average value of PLV for each subject, divided by signal pairs and frequency range. In each figure the PLV is computed for CRI and respiration (RESP), BVP and HRV signals respectively, from top to bottom.

In each figure the last four signals are highlighted in yellow: these represent subjects who

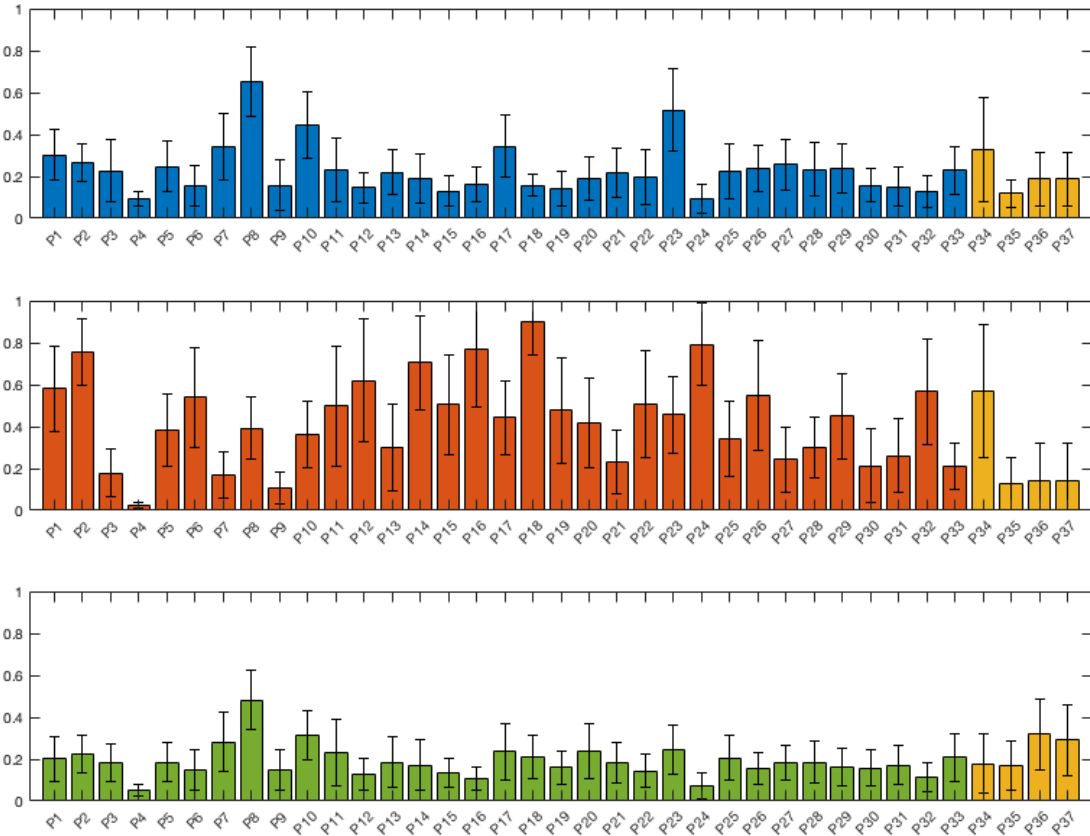


Figure 14 PLV of M-Band signals. Computed for CRI and respiration, BVP and HRV respectively.

were asked to maintain a state of apnea for a few seconds.

Starting from the PLV relative to the M-Band signals (Figure 14), it can be seen that some subjects show high correlation peaks, respectively 0.75 ± 0.2 for CRI-RESP, 0.49 ± 0.31 for CRI-BVP and 0.72 ± 0.15 for CRI-HRV. The most promising results regarding this metric are observed in this band. In the other two lower bands, the degree of correlation indicated by PLV is lower, as can be seen in Figure 15. The best data in these two bands is given by the CRI-RESP pair in VL band, with an average PLV value of $0.24 + 0.12$.

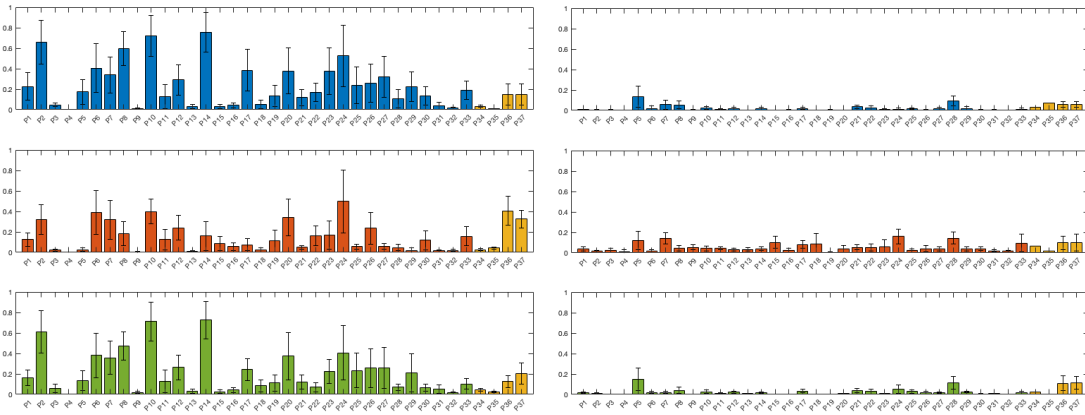


Figure 15 PLV of L-Band (left) and VL-Band (right) signals. Computed for CRI and RESP, BVP and HRV respectively.

4.5 Peak Detection on CRI Signal

Having established that among the various relationships of the CRI signal with the others, the strongest one seemed to be the one with the breath signal, the work went on to analyze the peaks of the CRI signal to try to see if there were any correlations with particular morphologies of the breath signal.

The analyses developed in this and the next section were designed with a view to determining, ideally, a possible way to obtain an indirect recording of the CRI signal.

It was therefore planned to work from the CRI signal, looking for certain peaks present on it, in order to obtain a "ground truth" on which to rely to validate a possible recognition technique based on the breath signal. The developed algorithm then goes to search for peaks on the CRI signal and create windows of the CRI and breath signals centered on them. Random windows on the breath signal are also selected. The process is explained in detail in Section 3.3.6.

The acquired windows are then to be cataloged into 9 clusters, to try to highlight common morphologies at the selected peaks. The results of clustering relative to the peaks are shown in Figure 17.

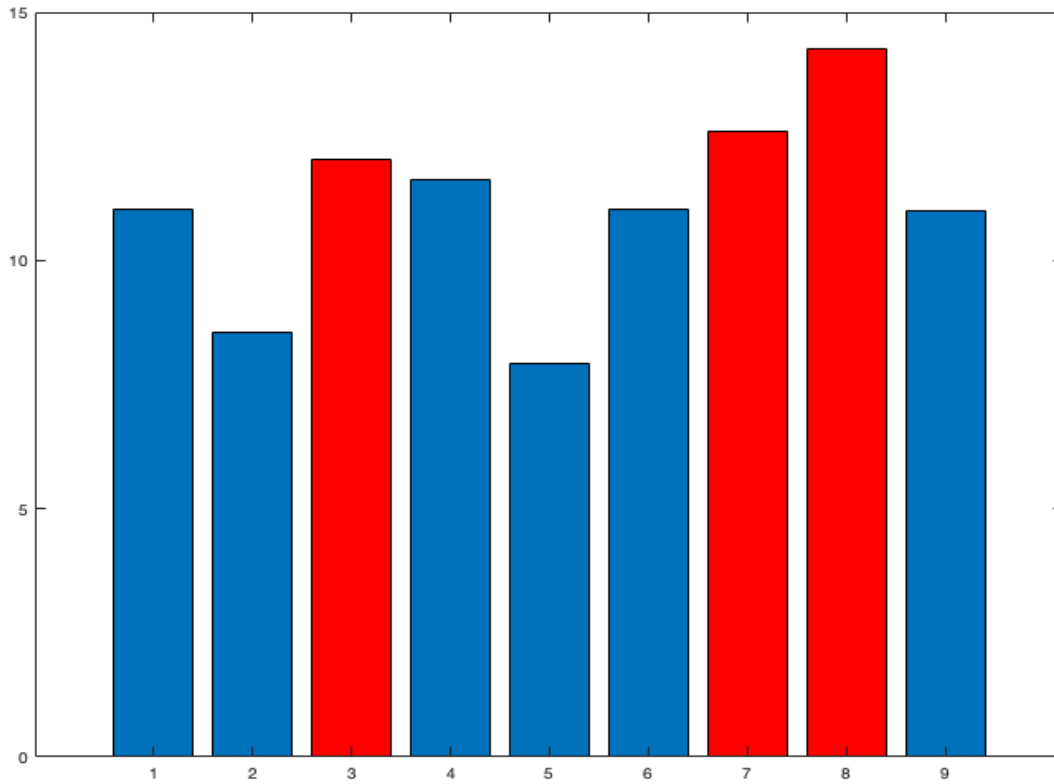


Figure 16 Bar diagram of each cluster population

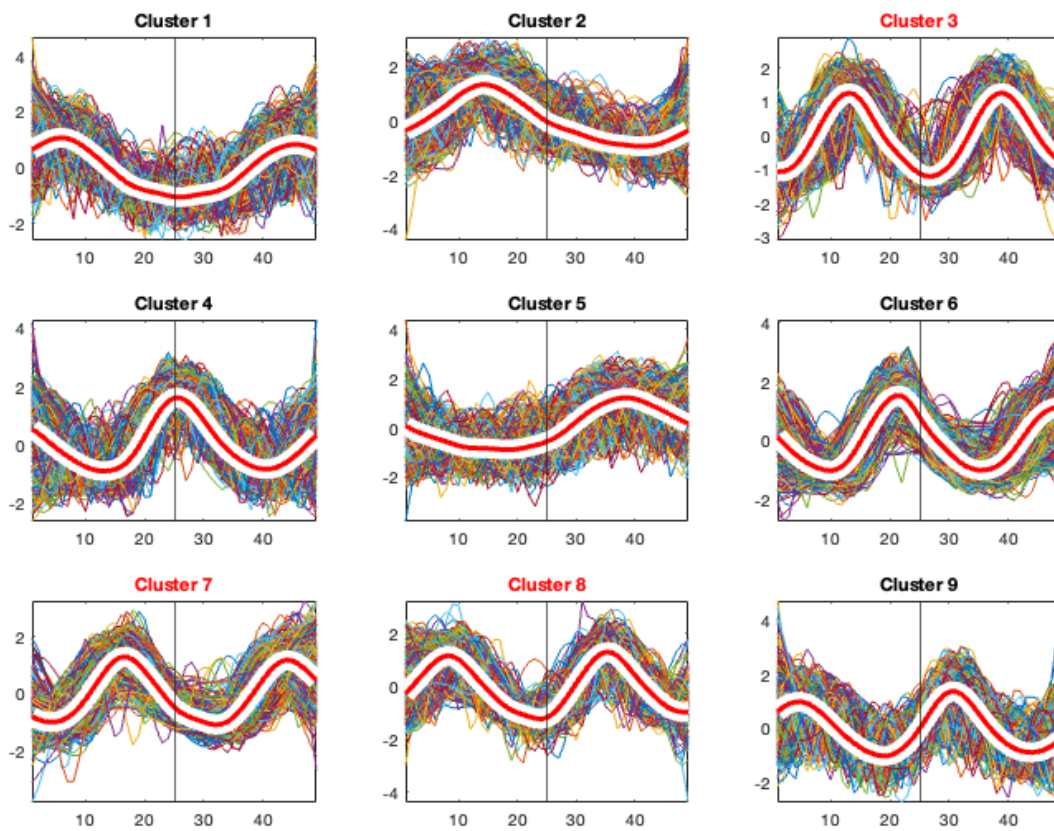


Figure 17 Clustering of RESP signal windows, centered on CRI signal peaks.

It can be seen from the figure above how in particular clusters 3, 7 and 8 show a similar respiratory wave pattern. Indeed it is evident, especially in cluster 7, how the peak detected on the CRI signal (indicated by the vertical line in the center of the graph) is at a change in steepness of the portion of the curve describing exhalation.

The clusters mentioned above are also the three most populated, as can be seen in Figure 16. The algorithm is able for any number of clusters chosen to fit and create plots with appropriate grids, as well as determine the correct number of clusters to select as most populated. This number is in fact defined as the square root of the number of clusters, in this case resulting to be three. The three most populated clusters in the case of breath signals centered on the peak of the M-band CRI signal (whose title and bar is highlighted in red) represent 38.7% of the population.

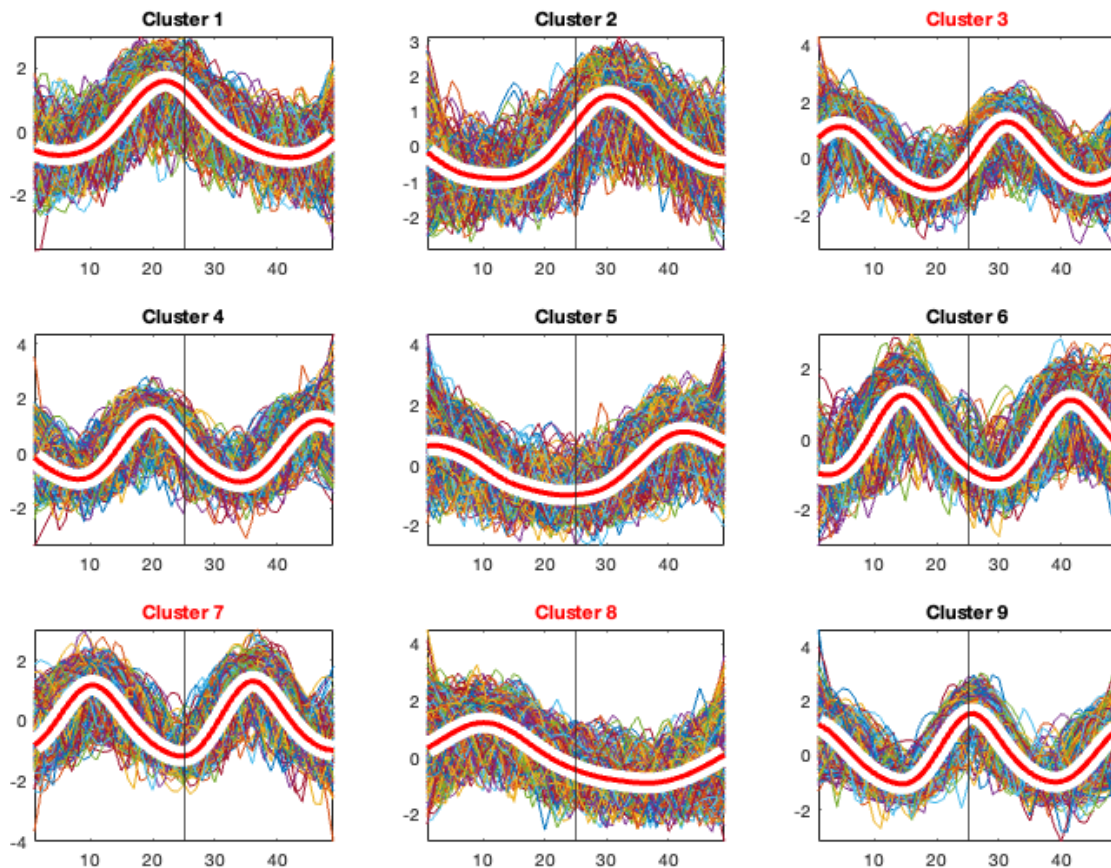


Figure 18 Clustering of random RESP signal windows

Looking at Figure 18, it is evident that even in this clustering in several signals show the same pattern evidenced in the three most populated clusters among those centered on the peaks. This phenomenon is particularly evident in clusters 4, 6 and 7 related to Figure 18. The fact that clustering on random windows shows markedly similar behavior to clustering centered on CRI signal peaks (three clusters with the same shape in both cases) demonstrates that the correlation between CRI peaks and respiratory signal morphology is not strong enough to statistically define a connection.

The results obtained up to this point from clustering the CRI spike-centered windows seemed quite promising, but unfortunately the considerations made about random windows did not make it possible to validate this technique for extrapolating the CRI rhythm from the breath signal.

4.6 Peak Detection on Respiration Signal

Continuing with the search for a possible correlation between breath signal and CRI, an inverse approach to the previous one was attempted. It was chosen for this analysis to start from the search for particular morphologies on the breath signal, and to investigate their possible correlation to events on the CRI trace.

The search for these anomalies started after an extensive observation phase of the traces related to the subjects' respiratory signals, in which a particular behavior showing some repetitiveness was noted. The anomaly in question consisted of the presence of a local minimum in the typically monotonic decreasing phase related to exhalation.

The search for these anomalies, was implemented at a preliminary stage with a simple search for local minima with specific parameters. Later, given the variability in the morphology of these anomalies, more sophisticated methodologies were considered: the choice fell on the *deepSignalAnomalyDetector* package, recently added to MATLAB's Deep Learning toolbox.

The results obtained with this deep learning technique, explained in more detail in section 3.3.7, are promising, as can be observed in Figure 19 and Figure 20.

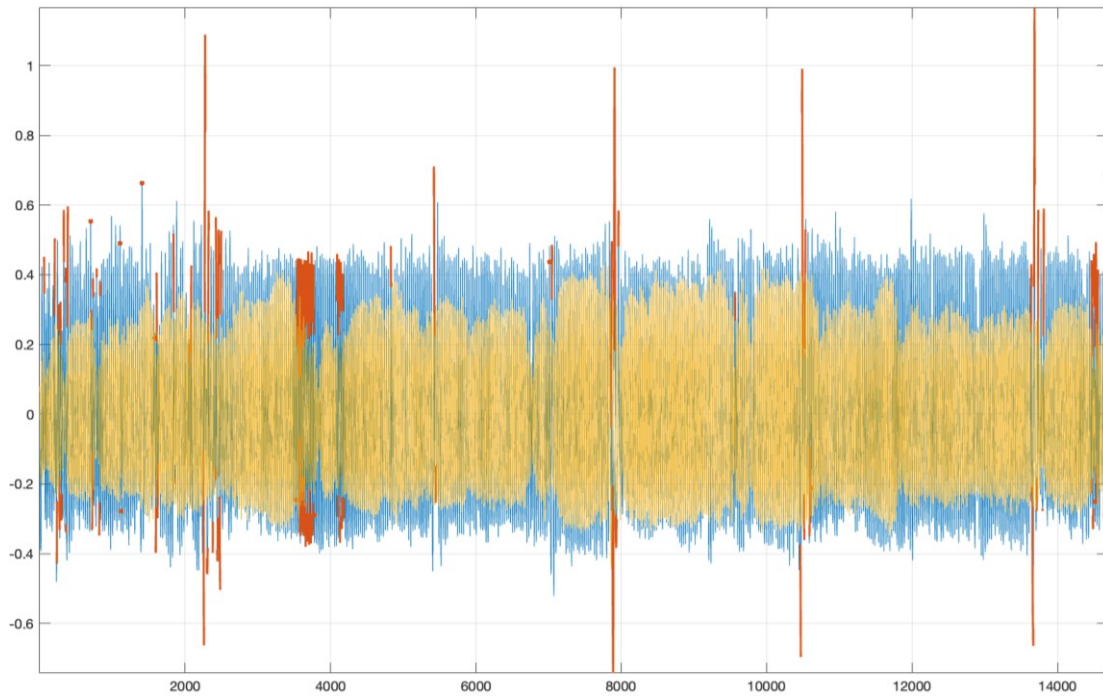


Figure 19 Output from deepsignalanomalydetector, showing original RESP signal (in blue), reconstructed signal (in yellow) and detected anomalies (in red).

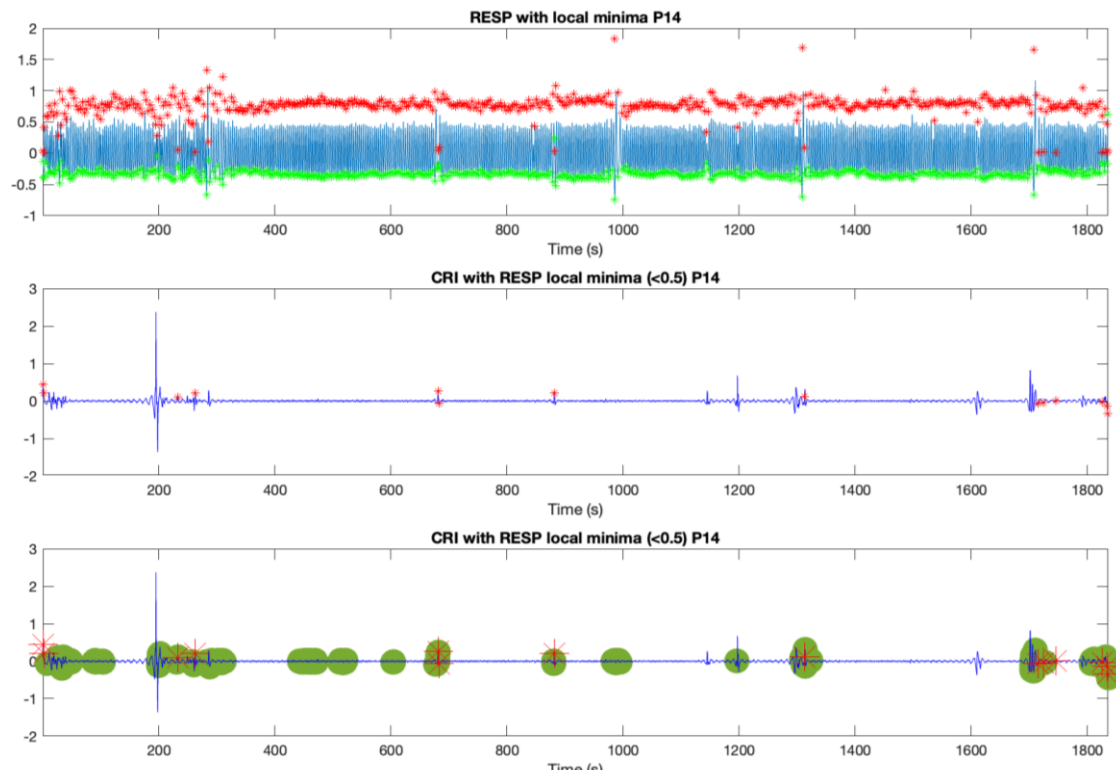


Figure 20 Combined Plot of RESP signal with local minima, as well as CRI signal with local minima and anomaly detected periods.

Specifically in Figure 20, it is possible to appreciate in the bottom graph how there is a good correspondence between the local minima found analytically and the abnormal zones detected by the deep learning algorithm.

Unfortunately, since we do not have a "ground truth" regarding the pulsations perceived by an osteopath, it is not possible to make an absolute validation of what is calculated through this analysis.

4.7 Granger Causality

A further approach to understanding the relationships between the available signals has been made in terms of the calculation of causality according to Granger.

The results for this analysis were unfortunately not found to be very consistent. In terms of the time domain, one of the most consistent data concerns the causal relationship between HRV and CRI (respectively 3 and 4 in the rightest plot), reported from the analysis of several subjects, as can be seen in Figure 21.

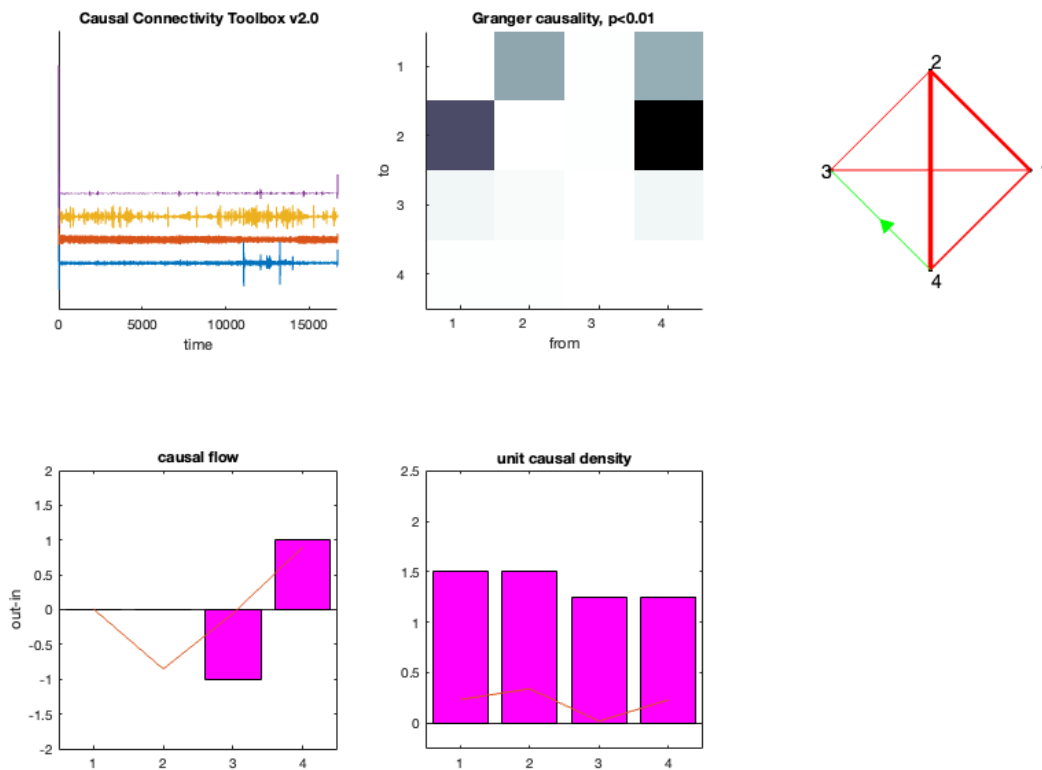


Figure 21 Time Domain Granger Causality analysis.

This analysis was conducted on a subgroup of patients whose signals seemed more promising and cleaner. The result regarding the connection between HRV and CRI appears to be quite consistent within these signals. However, it remains isolated from the results obtained from the other techniques, where on several occasions the strongest correlation was seen between the CRI and respiratory signals.

Additional metrics regarding Granger causality were calculated, such as causal flow, causal density and consistency, but the results obtained did not show relevant repetitiveness.

4.8 Magnitude Squared Coherence

One of the last measures to be implemented in the pipeline was Magnitude Squared Coherence. The calculation of this metric was done to look for possible frequency ranges in which a particular pair of signals might show signs of correlation.

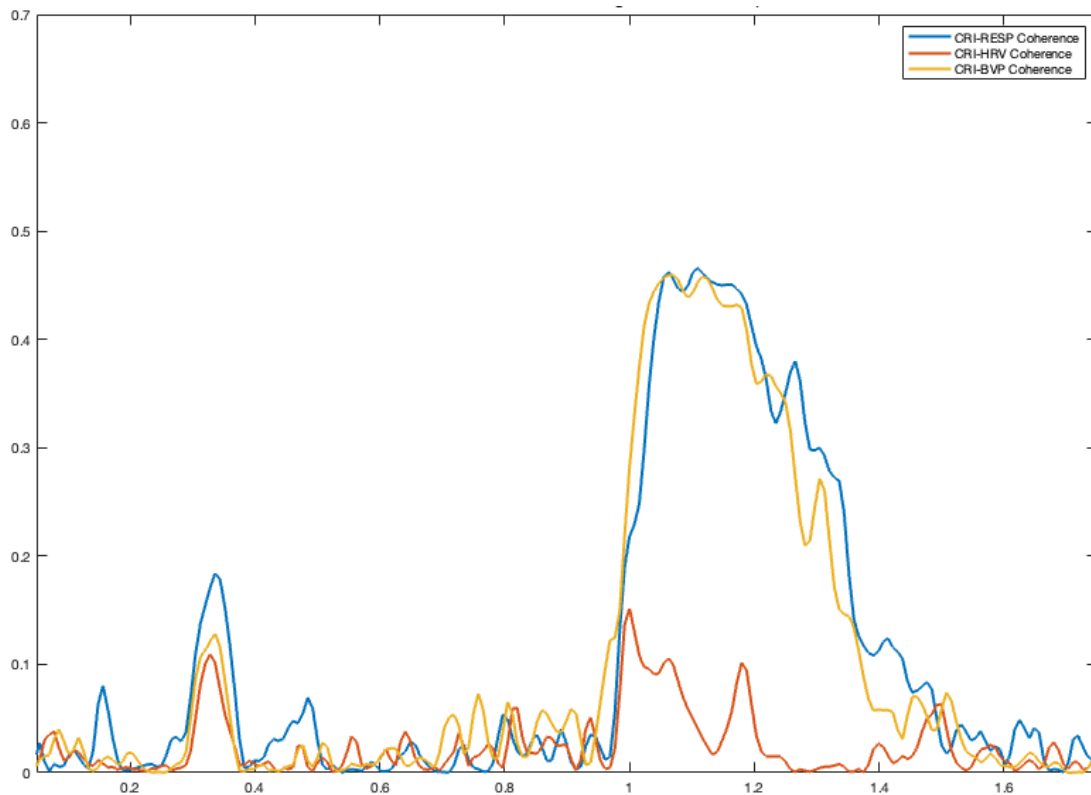


Figure 22 MS Coherence averaged over all subjects, relative to signals in M-Band.

This step may seem counterintuitive at this point in the analysis, but the sense with which it was integrated lies in the search for narrow bands with coherence peaks, on which to possibly focus to repeat previous analysis steps, the results of which did not yield positive outcomes because they were averaged over wider frequency bands.

As is clearly visible in Figure 22, this metric yielded the expected results. Clear coherence peaks can be seen around 0.3 and 1 Hz, ranges in which all signals show frequency content, influenced by respiration rate and the heart rate pulse. This consideration finds further support in the fact that the signal pairs with higher coherence are the ones in which the CRI signal is analyzed together with the BVP and respiration.

5 Discussion

5.1 Implications of Results

Although the results obtained from the different analysis techniques varied, it was possible to define and confirm some considerations regarding the CRI signal. It is evident from the results obtained that there is in fact a correlation between the signal recorded on the skull and the respiratory motion recorded on the chest. Unfortunately, it was not possible to precisely determine its physiological and analytical connection with the available data.

The conclusions drawn would suggest, as other authors have written before^{16,28}, that there is indeed a relationship between the pulmonary respiratory mechanism and that detected on the skull.

Further confirmation is that of the massive presence of BVP signal components within the one recorded with the cranial band. This phenomenon is partly explained by the general diffusion within the body of the pressure wave given by the heart rhythm, which affects almost all recordable parameters, albeit in different measures.

The discovery of a statistically significant correlation between CRI pulsation and another measurable parameter (possibly more conveniently) would give a breakthrough to osteopathy in the cranial field. In addition to confirming from the point of view of the scientific community the actual existence of rhythmic cranial motion, it would also make the process of measuring the latter much more objective, repeatable, and operator-free.

5.2 Limitations and Future Improvements

Among the biggest limitations of this work is definitely the lack of auxiliary data regarding the measurements made of the signals. On almost all the subjects there are small areas where some of the signals show markedly different trends from the norm and are out of scale. In all probability these points are related to times when the subject moved or the sensors were

touched, but unfortunately it was not possible to retrieve such information regarding the data acquisition. Regarding the alleged motion artifacts, an EMG signal would also have been valuable, so that it could be used to be able to exclude these segments.

Speaking more specifically about the CRI signal, a major lack in this dataset was definitely a signal related to palpation by an osteopath. The information that could have been obtained would have constituted ground truth that would have made the validation of the various analysis techniques much more accurate and faster.

Not mentioned in the previous chapter on results, one last step was implemented, designed as a possible starting point for possible future development of this project.

In fact, a section of code was written to perform denoising of signals using the spectral subtraction technique. Although in itself it did not return the hoped-for results, it was considered correct to include this last addition as well since it could lead to better results than those obtained in this study if used with other source data and developed more thoroughly.

In conclusion, although this work has not yielded the hoped-for results regarding a possible technique for objectively measuring the CRI signal, the statistics calculated on the available data certainly help to define this signal more and more clearly.

Precisely seeing the paucity of positive results obtained the MATLAB code developed, a central part of this work, has been made as general as possible, with the hope that it will form a solid basis to enable future work to reach where it was not possible with this present one.

Bibliography

1. W. G. Sutherland. *The Cranial Bowl*. (1939).
2. Haller, H. *et al.* Craniosacral Therapy for the Treatment of Chronic Neck Pain. *Clin J Pain* **32**, 441–449 (2016).
3. Green BHSc, C., Martin, C. W., Bassett, K. & Kazanjian Soc, A. *Systematically Reviewing Non-Randomised Controlled Trial Evidence on Complementary Medicine: A Health Technology Assessment Perspective*. www.chspr.ubc.ca (1999).
4. Kenneth E. Nelson, Nicette Sergueef, Celia M. Lipinski, Arina R. Chapman & Thomas Glonek. Cranial rhythmic impulse related to the Traube-Hering-Mayer oscillation: comparing laser-Doppler flowmetry and palpation. *JAOA* **101**, 163–173 (2001).
5. Nelson, K. E., Sergueef, N. & Glonek, T. *Recording the rate of the cranial rhythmic impulse*. Article in *The Journal of the American Osteopathic Association* <https://www.researchgate.net/publication/6992984> (2006).
6. Sergueef, N., Greer, M. A., Nelson, K. E. & Glonek, T. The palpated cranial rhythmic impulse (CRI): Its normative rate and examiner experience. *International Journal of Osteopathic Medicine* **14**, 10–16 (2011).
7. Moran, R. W. & Gibbons, P. Intraexaminer and interexaminer reliability for palpation of the cranial rhythmic impulse at the head and sacrum. *J Manipulative Physiol Ther* **24**, 183–190 (2001).
8. Halma et al • Original Contribution. *Intraobserver Reliability of Cranial Strain Patterns as Evaluated by Osteopathic Physicians: A Pilot Study*. (2008).

9. Hamm, D. A hypothesis to explain the palpatory experience and therapeutic claims in the practice of osteopathy in the cranial field. *International Journal of Osteopathic Medicine* **14**, 149–165 (2011).
10. Castejón-Castejón, M., Murcia-González, M. A., Todri, J., Lena, O. & Chillón-Martínez, R. Treatment of infant colic with craniosacral therapy. A randomized controlled trial. *Complement Ther Med* **71**, 102885 (2022).
11. Haller, H., Lauche, R., Sundberg, T., Dobos, G. & Cramer, H. Craniosacral therapy for chronic pain: a systematic review and meta-analysis of randomized controlled trials. *BMC Musculoskelet Disord* **21**, 1 (2019).
12. Liddle, S. D. & Pennick, V. Interventions for preventing and treating low-back and pelvic pain during pregnancy. *Cochrane Database of Systematic Reviews* **2015**, (2015).
13. Susha Cheriyeedath, M. Sc. Photoplethysmography (PPG). [https://www.news-medical.net/health/Photoplethysmography-\(PPG\).aspx](https://www.news-medical.net/health/Photoplethysmography-(PPG).aspx) (2019).
14. Bolanos, M. & Haltiwanger, E. *Comparison of Heart Rate Variability Signal Features Derived from Electrocardiography and Photoplethysmography in Healthy Individuals*.
15. Hopkins, J. Vital Signs. <https://www.hopkinsmedicine.org/health/conditions-and-diseases/vital-signs-body-temperature-pulse-rate-respiration-rate-blood-pressure#:~:text=Normal%20respiration%20rates%20for%20an,to%2016%20breaths%20per%20minute.>
16. Frymann, V. M. & La Jolla, F. *A study of the rhythmic motions of the Cranium living cranium*. (1971).
17. Rasmussen, T. R. & Meulengracht, K. C. Direct measurement of the rhythmic motions of the human head identifies a third rhythm. *J Bodyw Mov Ther* **26**, 24–29 (2021).

18. Cunningham, M. J. & Bibby Bsc, G. L. *Electrical Measurement*.
19. Najarian, K. & Splinter, R. *Second Edition Biomedical Signal and Image Processing*.
20. George W. Arnold *et al. Biomedical Signal Analysis*.
21. Kendall M. *Time-Series*. (Charles Griffin, 1976).
22. Challis, R. E. & Kitney, R. I. *Biomedical signal processing (in four parts)*. vol. 28 (1990).
23. Sheno, B. A. *Introduction to digital signal processing and filter design*. (Wiley, 2005).
24. Strada, M. & Cattaneo, R. *Respirazione Primaria*. (SOMA, 2020).
25. Seth, A. K. A MATLAB toolbox for Granger causal connectivity analysis. *J Neurosci Methods* **186**, 262–273 (2010).
26. Esfandiar Zavarehei. Berouti Spectral Subtraction.
27. Esfandiar Zavarehei. Boll Spectral Subtraction.
28. Ferguson, A. *A review of the physiology of cranial osteopathy*. *Journal of Osteopathic Medicine* vol. 6 (2003).

Acknowledgments

I would like to express my sincere gratitude to my thesis supervisor, Professor Mesin, for his unwavering support, patience, expert guidance, and encouragement throughout the research process. His insights and constructive feedback have been invaluable in shaping the direction and focus of this thesis.

I am also very grateful to my girlfriend Arianna, who has shown me her unceasing support throughout the academic journey over the past five years. Her presence, advice and cheerfulness have been among the most important cornerstones for me during this period, consisting of ups and downs that were less burdening thanks to her presence in my life.

Among all, I feel most grateful for my family. The all-around continuous support that my parents have provided me, not only during my university years, is of inestimable value. I would not have been able to achieve the goals I have without their help, encouragement, and example. A special mention goes to my uncle Franco, who walked these steps before me, and whose footsteps inspired me from an early age to follow this path.

A special thanks goes also to my dearest friends, whose company and support has been very appreciated in these years.

This thesis is a culmination of the collective support and contributions from these individuals and the institution of Politecnico di Torino. I am truly grateful for their impact on this academic endeavor.